

CHARACTERISTICS OF NAVY MEDIUM-WEIGHT HIGH-IMPACT SHOCK MACHINE

Robert W. Conrad

September 14, 1951

Approved by:

Dr. Irwin Vigness, Head, Shock and Vibration Branch
Dr. George R. Irwin, Superintendent, Mechanics Division



NAVAL RESEARCH LABORATORY

CAPTAIN F. R. FURTH, USN, DIRECTOR

WASHINGTON, D.C.

CONTENTS

Abstract	iv
Problem Status	iv
Authorization	iv
INTRODUCTION	1
THE MEDIUM-WEIGHT SHOCK MACHINE	1
LOADS AND MOUNTING ARRANGEMENTS	3
HAMMER DROP AND TABLE TRAVEL	4
INSTRUMENTATION	4
EQUIVALENT SINGLE-DEGREE-OF-FREEDOM SYSTEM	7
EXPERIMENTAL RESULTS	9
Anvil-Table Velocity - General	9
Initial Anvil-Table Velocity	10
Average Anvil-Table Velocity	10
Anvil-Table Reversal Velocity	14
Load Velocity - General	15
Peak-Load Velocity	16
Load Velocity Resulting From Table Reversal	18
Anvil-Table Acceleration - General	17
Peak Anvil-Table Acceleration	17
Anvil-Table Reversal Acceleration	20
Load Acceleration - General	21
Peak-Load Acceleration	21
Load Acceleration after Table Reversal	22
Load Frequency	23
Reed-Gage Data	23
Correlation between Theoretical and Experimental Results	23
SUMMARY	26
ACKNOWLEDGMENTS	27
REFERENCES	28
APPENDIX I - Descriptive Details of Mounting Arrangements	29
APPENDIX II - Derivation of Equations of Motion	29

ABSTRACT

A study was made of the Medium Weight High Impact Shock Machine to determine the magnitude, frequencies, and general characteristics of the shock developed by this machine under specification operation. A comparison of data is intended to correlate this shock to shipboard shock experienced in actual combat and to compare the shocks delivered by other machines of a similar type.

Records were made of the motions on the load and on the anvil table for four types of loading, for three distances of anvil-table travel, and for hammer drops corresponding to Class A and B tests of standard military specifications (9) plus additional blows equivalent to 150 percent of Class A and 50 percent of Class B blows. Both bolt-spacing distances allowed by the rectangular load dimensions were tested for each load weight, resulting in a total of eight distinct runs.

Relationships between peak measurements of acceleration and velocity on the anvil table and load are shown to be linearly related to the hammer impact velocity. Motions resulting from anvil-table reversal are discussed, and it is shown that this secondary shock can be the largest under certain conditions. Theoretical equations of motion are developed and their correspondence to experimental data demonstrated.

PROBLEM STATUS

This is an interim report; work on this problem is continuing.

AUTHORIZATION

NRL Problem 38F03-38P

ADB NS-711-101

Manuscript submitted for publication: June 13, 1951

CHARACTERISTICS OF NAVY MEDIUM-WEIGHT HIGH-IMPACT SHOCK MACHINE

INTRODUCTION

The importance of protecting naval shipboard equipment from damage caused by near misses, noncontact explosions, concussion from the ship's own guns, as well as damage from direct hits in adjacent spaces was recognized shortly after the close of World War I. Since then, technical advances in weapons and missiles, and increased reliance on delicate, complex equipment has made the shock-protection program of vital interest to the Navy. Numerous shock and vibration machines have been constructed to simulate, in the laboratory, the type and magnitude of shock motions encountered under combat conditions. These machines then served as a basis of acceptability for numerous shipboard equipments and were also used to point out inherent design weaknesses.

Considerable study has been made recently of the shock machines in common use to compare them with one another and with field conditions, so that unnecessary duplications may be eliminated and more realistic tests employed. The 250 Ft-lb Shock Machine (1), the 3 Ft-lb Vibration Machine (2), and the Shock Machine for Electronic Devices (3, 4, 5) have been investigated and reports written covering their characteristics. The few reports on the Medium-Weight High-Impact Shock Machines (6) and the Light-Weight High-Impact Shock Machines (7,8) have dealt mainly with their special attributes and have not attempted to cover their characteristics over their entire operating range. Changes in mounting arrangements and machine modifications have been made as the needs became apparent, necessitating a reinvestigation of the machine characteristics under these new conditions.

This report covers an investigation of the Medium-Weight Shock Machine when loaded and operated in accordance with the governing shock-test specifications (9, 10). Experimental test runs were begun on 24 February 1950 and completed 21 August 1950. Two preliminary letter reports covering loads, mounting arrangements, and instrumentation (11), and peak shock motions (12) have been submitted to BuShips to expedite the release of this information. This report now summarizes all these data in one coherent document.

THE MEDIUM-WEIGHT SHOCK MACHINE

The NRL Medium-Weight Shock Machine, one of the latest versions of this type, was first put into operation in the latter part of 1946. Incorporating all operational features and conveniences lacking in the original installation at the Engineering Experiment Station, it includes pneumatic table jacks, base restraints, and the quick-release mechanism. Shortly after being put into operation, difficulty was experienced in keeping the anvil-table hold-down bolts tightened, despite the use of lock nuts. This trouble was

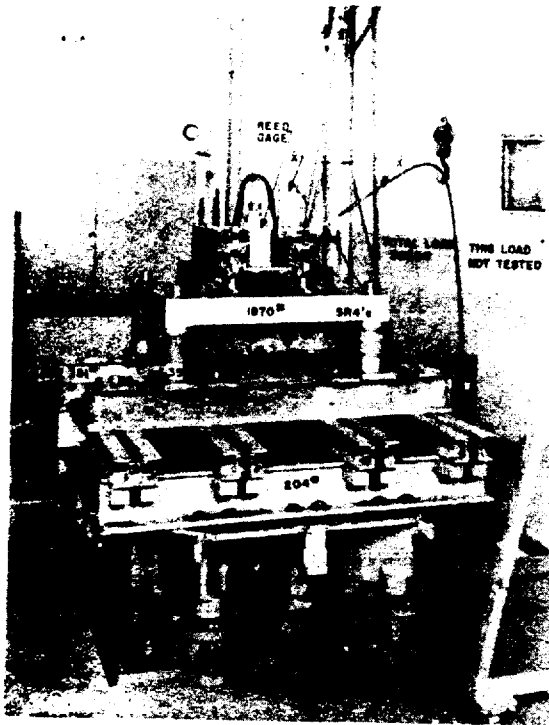


Figure 1 - Experimental test setup for Run 5. (Note the reinforcing pads welded to the anvil-table stiffeners.)

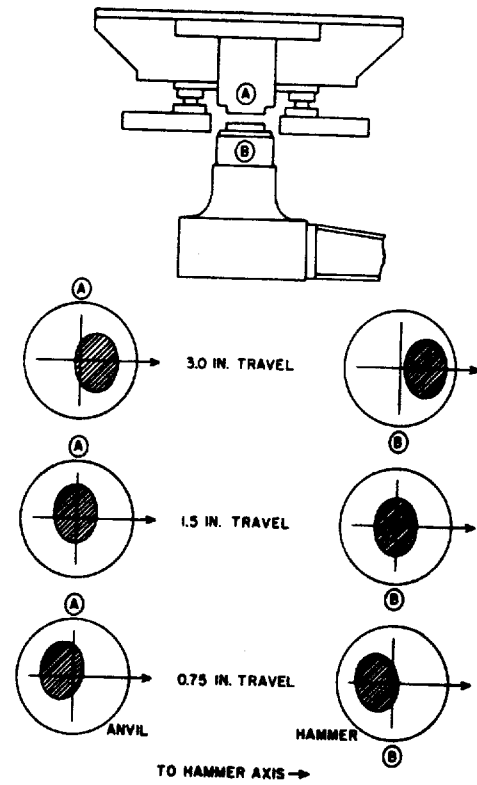


Figure 2 - Hammer and anvil contact areas

remedied, however, by pinning both the nut and the lock nut to the hold-down bolt. In October 1948, cracks were noted in the anvil-table reinforcing webs, which bore against the pneumatic jacks. The cracks were longer on the webs which faced the hammer. Apparently, the anvil table often assumed a decided tilt so that the landing shocks were absorbed by the webs striking the jack body rather than being absorbed by the ring pads. Repairs were made on the cracked members by welding 14 in. x 4 in. x 7/8 in. steel pads on both sides across the cracks and by welding an 8-1/2 in. x 4 in. x 1-1/4 in. steel pad along the bottom. About a year later, similar cracks were noted in webs which had not been reinforced, the worst cracks again being found in the webs which faced the hammer. Identical reinforcing pads (Figure 1) were then welded to all remaining webs, and the entire anvil-table assembly stress relieved.

No quantitative data are available which would permit a comparison of the anvil-table stiffness before and after addition of the reinforcing pads; the change probably was negligible. Addition of the steel pads to all twelve webs, however, increased the anvil-table weight, including hold-down bolts and stop ring, to 4500 lb. This additional weight (12 percent) to the anvil table is probably reflected in a slightly less severe shock to equipment under test over that previously delivered.

An interesting operational feature of the machine was encountered while checking some of the experimental data. Paper targets were attached to both the hammer and anvil surfaces with the centers and orientations suitably marked to determine the contact areas. Carbon paper secured over the targets left prints of the contact areas on

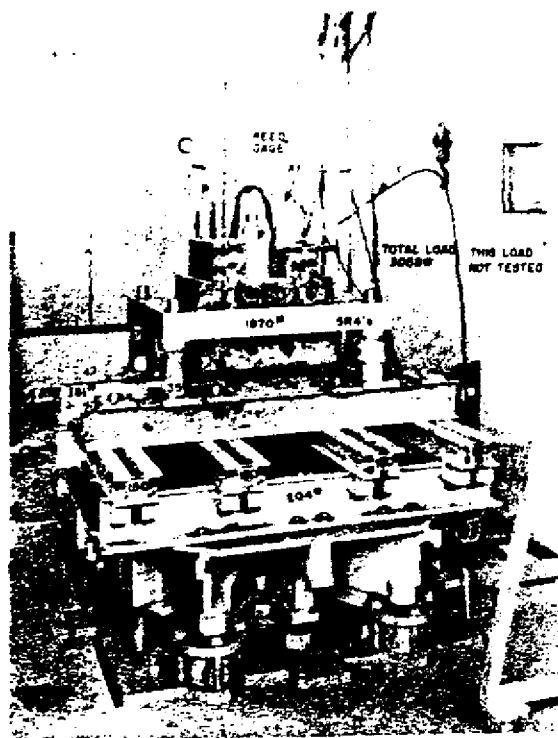


Figure 1 - Experimental test setup for Run 5. (Note the reinforcing pads welded to the anvil-table stiffeners.)

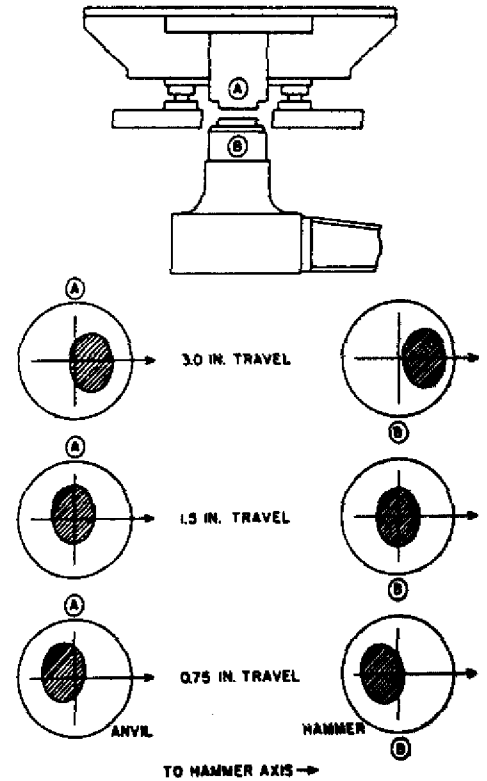


Figure 2 - Hammer and anvil contact areas

remedied, however, by pinning both the nut and the lock nut to the hold-down bolt. In October 1948, cracks were noted in the anvil-table reinforcing webs, which bore against the pneumatic jacks. The cracks were longer on the webs which faced the hammer. Apparently, the anvil table often assumed a decided tilt so that the landing shocks were absorbed by the webs striking the jack body rather than being absorbed by the ring pads. Repairs were made on the cracked members by welding 14 in. x 4 in. x 7/8 in. steel pads on both sides across the cracks and by welding an 8-1/2 in. x 4 in. x 1-1/4 in. steel pad along the bottom. About a year later, similar cracks were noted in webs which had not been reinforced, the worst cracks again being found in the webs which faced the hammer. Identical reinforcing pads (Figure 1) were then welded to all remaining webs, and the entire anvil-table assembly stress relieved.

No quantitative data are available which would permit a comparison of the anvil-table stiffness before and after addition of the reinforcing pads; the change probably was negligible. Addition of the steel pads to all twelve webs, however, increased the anvil-table weight, including hold-down bolts and stop ring, to 4500 lb. This additional weight (12 percent) to the anvil table is probably reflected in a slightly less severe shock to equipment under test over that previously delivered.

An interesting operational feature of the machine was encountered while checking some of the experimental data. Paper targets were attached to both the hammer and anvil surfaces with the centers and orientations suitably marked to determine the contact areas. Carbon paper secured over the targets left prints of the contact areas on

as prescribed by the governing specifications. Support channels were used in pairs, back-to-back, spaced apart, and bolted together at the ends. The load was secured by T-clamps and mounting pads were supplied as required. Inasmuch as the physical arrangement of the support channels affects the results somewhat, this information has been placed in Appendix I.

TABLE I
Summary of Test Conditions

Run No.	Bolt Spacing (in.)	Load Weight (lb)	No. of Support Channels	Support Channel Weight (lb)	Total Weight on Anvil Table (lb)
1	16	1115	4	300	1858
2	24	1115	3	225	1783
3	16	2051	6	450	3026
4	24	2051	5	375	2951
5	24	3386 [†]	8	600	4420
6	32	3386 [†]	5 [‡]	375	4204
7	24	4423 [‡]	10	750	5616
8	32	4423 [‡]	7	525	5391

*Includes weight of base channels (408 lb) and instruments (35 lb).

†Includes weight of mounting pads (82 lb) across channels.

‡Includes weight of auxiliary channels (362 lb).

§Six support channels should have been used.

HAMMER DROP AND TABLE TRAVEL

Heights of hammer drop and distance of table travel were as specified for Class A and B equipment (9, 10), but with additional blows representing 50 percent of the height of drop specified for Class B equipment and 150 percent of that specified for Class A equipment. Exceptions were made to these conditions when the heights of drop were nearly equal for the same table travel or when they exceeded the machine capacity. A second departure from standard test procedure was introduced by including blows delivered with table travel restricted to 0.75 inch. Following the notation employed by the specifications, the 0.75-in. anvil-travel blows were designated as Group IV blows and were identical to Group III blows in all other respects. Height of hammer drop and anvil-table travels used during each run are given in Table 2.

INSTRUMENTATION

Shock motions of the anvil-table load were measured by two groups of instruments, each comprising an accelerometer, a velocity meter, and a multifrequency reed gage. A set of bonded wire resistance strain gages, cemented to one of the load-supporting feet, indicated the force exerted by the load on the supporting channels. Positions of the various pickups may be seen from Figures 1 and 4. With the exception of the reed gages the pickups generated an electrical signal in proportion to the characteristic they measured. Output signals were simultaneously recorded photographically by a five-channel cathode-ray-oscillograph assembly (Figure 5) and by a Mirragraph system for convenience of a later electrical analysis.

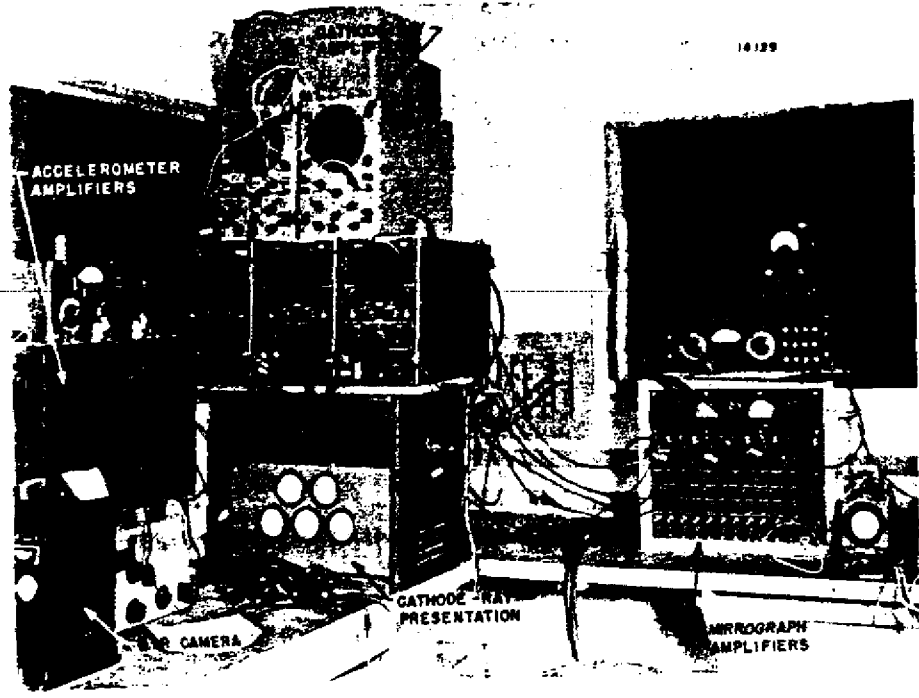


Figure 5 - Instrumentation setup in shielded room

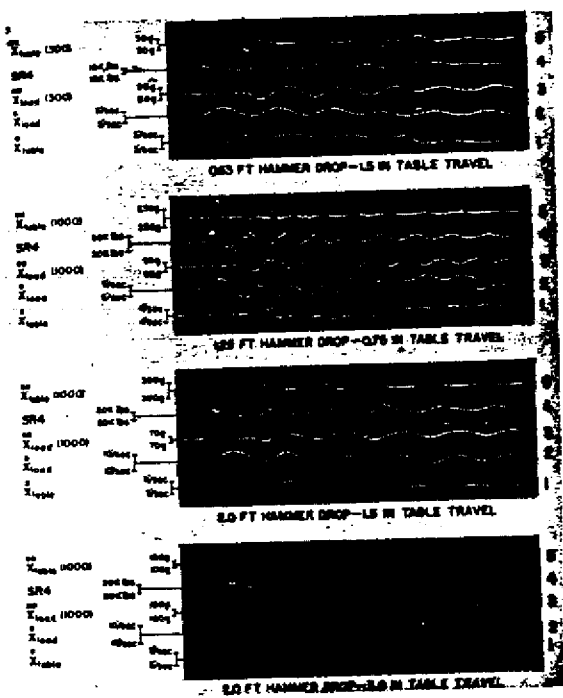


Figure 6 - Typical test records - Run 1
 Load weight, 115 lb
 Bolt spacing, 16 in.
 No. channels, 4

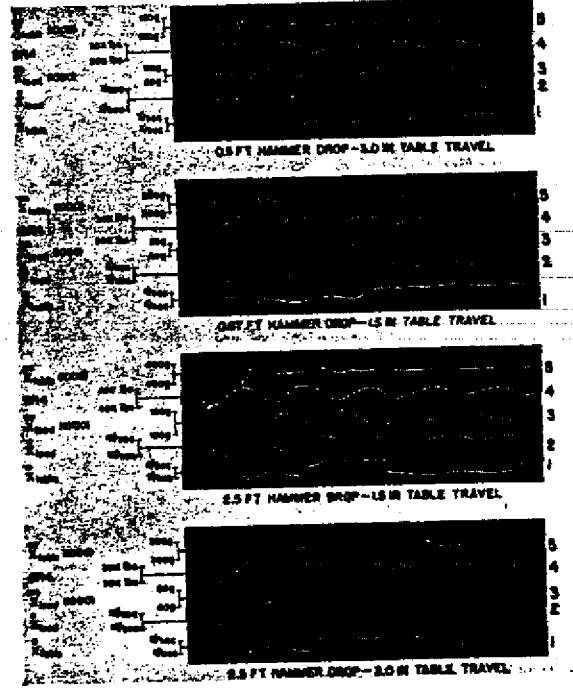


Figure 7 - Typical test records - Run 4
 Load weight, 2051 lb
 Bolt spacing, 24 in.
 No. channels, 5

TABLE 2
Height of Hammer Drop and Anvil-Table Travel

Group and Table Travel	Type of Test	Height of Hammer Drop (Feet)									
		Run 1	Run 2	Run 3	Run 4	Run 5	Run 6	Run 7	Run 8	Run 9	Run 10
Group I (3-in. table travel)	Class A	1.00	1.00	1.30	1.50	2.00	2.00	2.50			
	Class B	0.75	0.75	1.00	1.00	1.25	1.25	1.75			
	50% Class B	0.38	0.38	0.50	0.50	0.63	0.63	0.87			
Group II (3-in. table travel)	150% Class A	3.00	3.00	3.75	3.75	5.2	4.88				
	Class A	2.00	2.00	2.50	2.50	3.50	3.25	5.50			
	Class B	1.25	1.25	1.75	1.75	2.25	2.25	2.75			
Groups III and IV (1.5- and 0.75-in. table travel, respectively)	150% Class A	3.00	3.00	3.75	3.75	5.2	4.88				
	Class A	2.00	2.00	2.50	2.50	3.50	3.25	5.50			
	Class B	1.25	1.25	1.75	1.75	2.25	2.25	2.75			
	50% Class B	0.63	0.63	0.87	0.87	1.12	1.12	1.37			

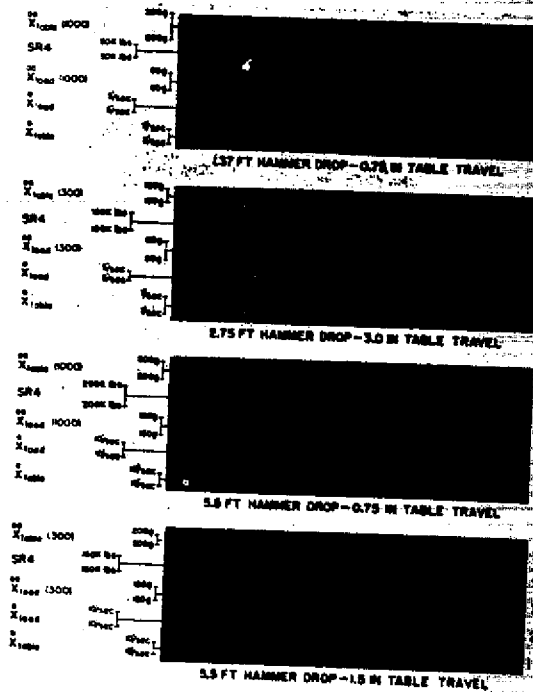


Figure 8 - Typical test records - Run 8
Load weight, 4423 lb
Bolt spacing, 32 in.
No. channels, 7

Table 3
Correlation of Pickup Type and Location

Test No.	Instrument	Experimental Location
1	Velocity Meter	Anvil-Table
2	Velocity Meter	Load
3	Accelerometer	Load
4	Strain Gage	Mounting-Boots
5	Accelerometer	Anvil-Table

Typical oscillographic test records are shown in Figures 6 through 8; Table 3 lists the measuring instrument with its experimental location and its position on the test record. Traces are numbered from the bottom up.

The recording arrangement did not permit a direct comparison of instantaneous signals until allowances were made for the displacements of the time scales for traces 2 and 4 (Figure 6) and the electrical delay occasioned by the low-pass filters on traces 3 and 5. These time displacements were constant and known for a given filter, and they were taken into consideration in establishing a time correspondence between traces.

Pickup units used during this investigation were standard types whose characteristics and limitations are well known. The velocity meter on the anvil table was an MB type 200, modified to reduce the natural frequency to about 2.5 cps. A Hartz Velocity Meter measured the load velocity, since this instrument can accommodate a larger displacement before bottoming and is consequently more satisfactory for electrical analysis. Westinghouse quartz-crystal accelerometers were secured to both the anvil table and load positions. Special precautions were observed to minimize disturbances from "cable microphonics" by using graphite-impregnated cable* and by supporting it independently from the shock table. Accelerometer signals were limited in frequency by a 300- or a 1000-cps low-pass filter to eliminate the high-frequency components which so often obscure the desired signals. Strain-gage elements were arranged as opposite arms of a bridge to eliminate bending stresses from the output. Both the velocity signals and strain-gage signals were recorded without filtration.

EQUIVALENT SINGLE-DEGREE-OF-FREEDOM SYSTEM

For study of anticipated shock motions, the shock machine and its load may be considered as a single-degree-of-freedom system, with the configuration given by Figure 9.

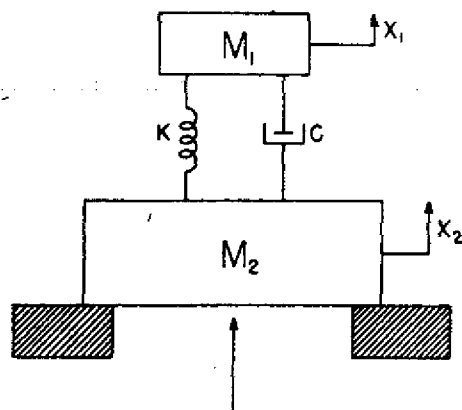


Figure 9 - Equivalent single-degree-of-freedom system

The load and anvil table were denoted as masses M_1 and M_2 , respectively, both assumed to be rigid bodies. The supporting channels were represented as a massless, linear spring with stiffness k and a viscous damping coefficient c . As a first approximation, the effects of gravity were neglected. Boundary conditions were chosen so that the entire system was at rest prior to $t = 0$, when the anvil table M_2 suddenly acquired a positive (upward) velocity V_0 . The initial acceleration of M_2 was assumed to occur in an interval which was negligibly short compared to the natural period of the system so that M_2 could be assumed to experience a step change in velocity.

The fundamental force equations for this system are:

$$\begin{aligned} -k(x_2 - x_1) - c(\dot{x}_2 - \dot{x}_1) &= M_2 \ddot{x}_2, \\ k(x_2 - x_1) + c(\dot{x}_2 - \dot{x}_1) &= M_1 \ddot{x}_1. \end{aligned}$$

* Graphite between the shield and the insulator and around the central conductor of a single-conductor shielded cable eliminated the effects of electrical charges building up on the surface of the insulator.

which are simultaneous, linear, differential equations that may be solved by ordinary methods. Equations of motion for both bodies, as derived in Appendix II, are given by the following expressions when the percent of critical damping is small:

$$x_1 = \frac{V_0}{1+m} \left[t - \frac{e^{-\frac{c}{c_c} \omega t}}{\omega} \sin \omega t \right] \quad x_2 = \frac{V_0}{1+m} \left[t + \frac{m e^{-\frac{c}{c_c} \omega t}}{\omega} \sin \omega t \right]$$

$$\dot{x}_1 = \frac{V_0}{1+m} \left[1 - e^{-\frac{c}{c_c} \omega t} \cos \omega t \right] \quad \dot{x}_2 = \frac{V_0}{1+m} \left[1 + m e^{-\frac{c}{c_c} \omega t} \cos \omega t \right]$$

$$\ddot{x}_1 = \frac{V_0 \omega}{1+m} \left[e^{-\frac{c}{c_c} \omega t} \sin \omega t \right] \quad \ddot{x}_2 = \frac{V_0 \omega}{1+m} \left[m e^{-\frac{c}{c_c} \omega t} \sin \omega t \right]$$

where $m = M_1/M_2$, the mass ratio,

$\frac{c}{c_c}$ = percent of critical damping,

$\omega = \sqrt{\frac{(M_1 + M_2)k}{M_1 M_2}}$, the reaction oscillation frequency, and

V_0 is the initial velocity acquired by M_2 .

Representative plots of these equations are shown (Figure 10) for c/c_c equal to 0.05 and gravity neglected. Curves for anvil-table displacement and velocity are shown for the approximate maximum and minimum values of mass ratio used experimentally. Some fundamental aspects of the shock motion are disclosed by this idealistic system. At the start the anvil table owns all the momentum in the system and the load is at rest. As time progresses, these bodies execute a sinusoidal interchange of momentum at a frequency determined by their individual masses and the channel stiffness. After an extended period determined by the damping coefficient, they will again reach equilibrium, each possessing a velocity of $V_0/(1+m)$. If gravity is considered, a velocity equal to g must be subtracted from the calculations. The two rigid bodies are 180 degrees out of phase, the relative acceleration amplitudes being governed by $\ddot{x}_2 = m \ddot{x}_1$. Addition of gravity produces a negligible zero shift in these plots.

In actual practice, one of two events occurs which determines whether the motions are as indicated. If the initial anvil-table velocity is not sufficient to cause the anvil table to reach its upper limit stops, the table rises until it expends its initial energy and then falls under the influence of gravity. No new transients are introduced until the anvil table

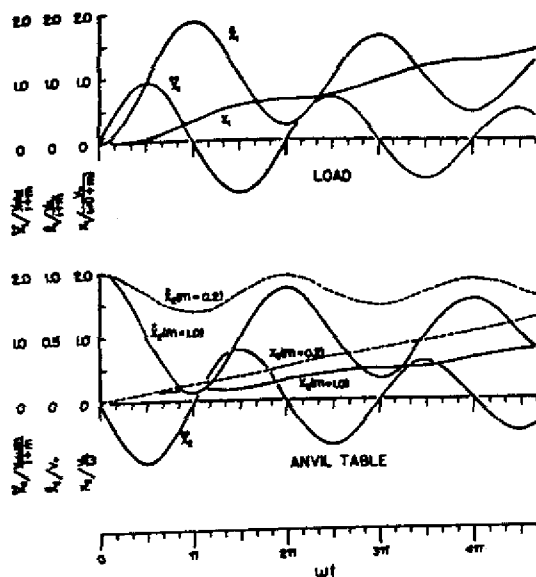


Figure 10 - Motions of equivalent system to a step-velocity change

assuming that the anvil-table velocity reverses abruptly to one half of its striking velocity. Although these restrictions prevent a direct comparison between theoretical and experimental results, they permit an insight into the mechanisms involved. Assume that the system of Figure 9 is initiated and allowed to run for a time τ , at which time the anvil-table velocity reverses. The new boundary conditions are then determined by the motions of the anvil table and load evaluated at τ . As shown by Appendix II, the load velocity is described by

$$\dot{x}_1 = \frac{V_0}{1+m} \left[(\sin \tau) \sin \omega t + (1 - \cos \tau) \cos \omega t \right] + \frac{V_0}{(1+m)^2} \left[m - \frac{1}{2} - \frac{3m}{2} \cos \tau \right] (1 - \cos \omega t).$$

A plot of this expression (Figure 11) is shown for a mass ratio of zero with τ as the variable. As one would expect, the maximum load velocity change results from anvil-table reversal, occurring when the load has its maximum velocity away from the anvil table (curve 3). Under these conditions, the magnitude of the reversal velocity change is larger than that caused by the initial hammer impact over most of the range and may reach a ratio of 2.5. In practice, however, ratios of this size never are encountered.

EXPERIMENTAL RESULTS

Anvil-Table Velocity - General

The anvil-table velocity waveform is characterized by features which are little affected by height of hammer drop, anvil-table travel, or load. It is a superposition of five major elements, viz, the initial-velocity change owing to hammer impact, a local high-frequency vibration of 750 cps caused by the anvil table vibrating as an elastic body, a

bottoms. The other alternative occurs when the anvil-table initial velocity is sufficient to allow it to reach its upper limit of travel. The anvil-table motion is abruptly reversed and a new set of transients are introduced which may nullify or augment the oscillations already in progress. Test parameters, i.e., anvil-table travel, initial velocity, natural frequency, and mass ratio, play an important role in determining the oscillation phase at reversal, and, therefore, the magnitude of the subsequent motions. A study of the load motions under the latter conditions is extremely important from the standpoint of shock damage and in the analysis of records from instruments such as the reed gage, which has no time-axis.

If some simplifying assumptions are made, a mathematical expression may be derived which includes the motions caused by anvil-table reversal. These include neglecting gravity, damping, and

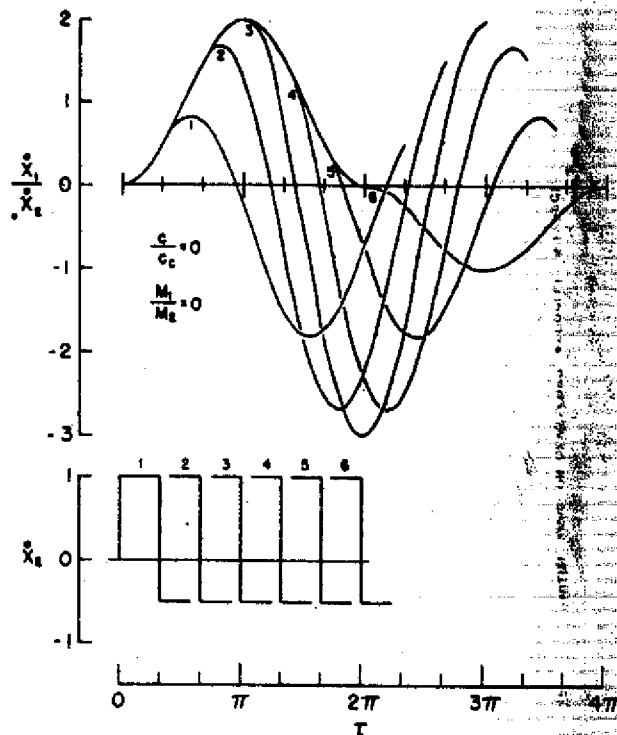


Figure 11 - Motion of equivalent system to a reversal-step change in velocity at any time after starting

low-frequency oscillation resulting from reaction of the load,* the retarding effect of gravity, and a velocity reversal if the anvil table strikes its upper limit stops. For the majority of blows the anvil table suffers three step-velocity changes caused by hammer impact, anvil-table reversal, and the final landing, which is negligible compared to the first two and usually ignored. Relative magnitudes between hammer impact and changes in anvil-table reversal velocity depend largely on the phase of the reaction component at the time of reversal.

Initial Anvil-Table Velocity

As a result of the hammer impact, the anvil table is accelerated for about one millisecond (Figure 3) while elastic vibrations of the anvil table are excited. Since the time of hammer-anvil contact is longer than half the natural period of the anvil table, the vibration builds up so that the first peak never is as large as the second. The amplitude of the first peak closely approximates the center line of the subsequent elastic vibrations, so that it is taken as the magnitude of the initial anvil-table velocity step. Plots of initial anvil-table velocity thus obtained for each experimental run are shown in Figures 12 through 19. As was noted with previous shock machines investigated, the initial anvil-table velocity is apparently a linear function of the hammer velocity (momentum) at impact, and, because of the resilience of the support channels, it is independent of the weight of the attached load. Slopes of these data plotted against hammer-impact velocity ranged from 0.58 down to 0.49, both extremes occurring during medium-load runs. The average slope of 0.54 was taken as the most probable value for the hammer-to-anvil-velocity transfer characteristic for channel-mounted loads. Loads rigidly mounted to the anvil table will alter this factor through their influence on anvil-table weight. The initial anvil-table velocity for a channel-supported load varied between 3.4 ft/sec for the lowest Class B blow of 0.75 ft up to 10.3 ft/sec for the maximum hammer drop of 5.5 ft. Figure 20 shows a combined plot of initial anvil-table velocities for all experimental runs and the maximum deviation from the average encountered during this investigation.

Average Anvil-Table Velocity

Three methods were available for evaluating the average anvil-table velocity, two based on experimental measurements, and the third derived from theoretical considerations.

*The reaction oscillation frequency is the natural frequency of the load on the support channels as defined by ω (page 8).

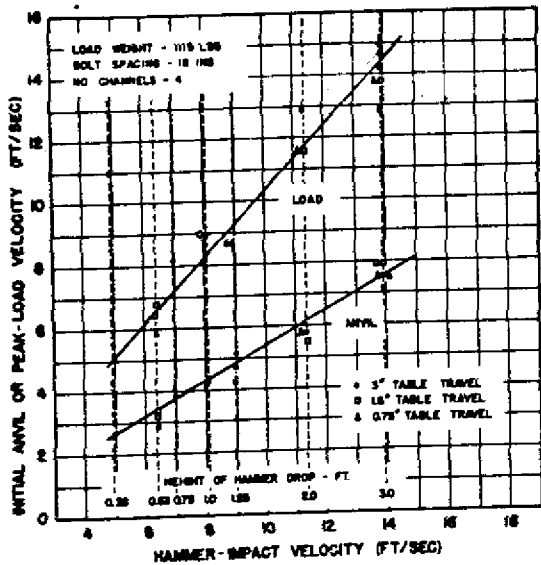


Figure 12 - Initial anvil-table velocity and peak-load velocity - Run 1

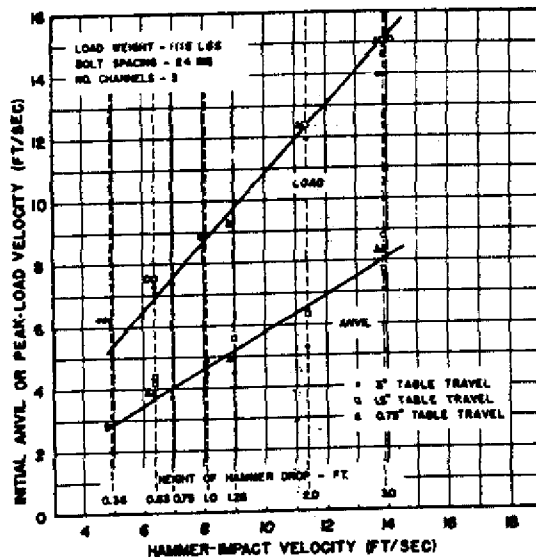


Figure 13 - Initial anvil-table velocity and peak-load velocity - Run 2

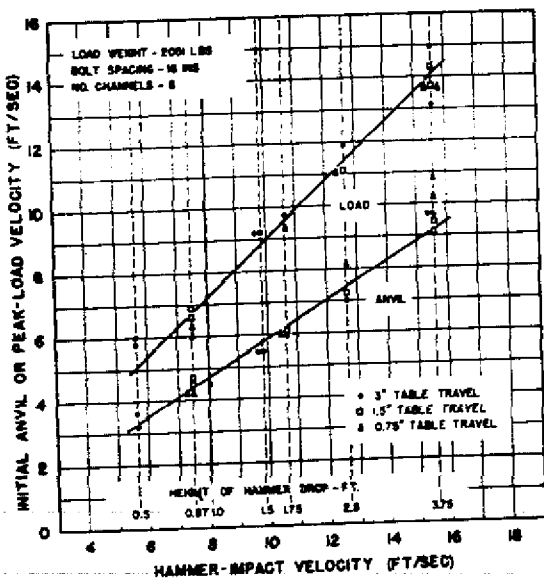


Figure 14 - Initial anvil-table velocity and peak-load velocity - Run 3

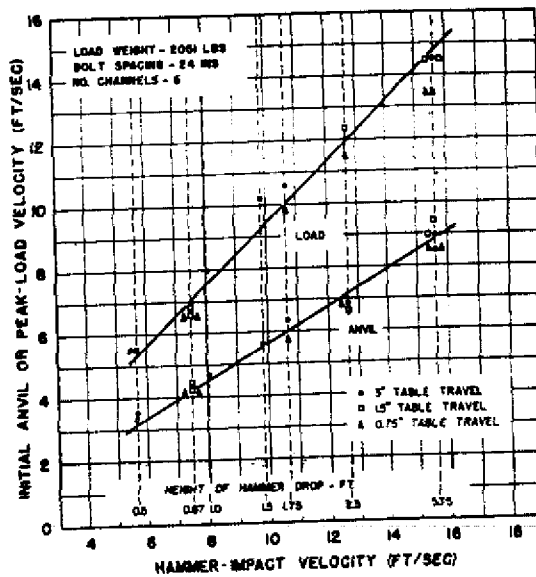


Figure 15 - Initial anvil-table velocity and peak-load velocity - Run 4

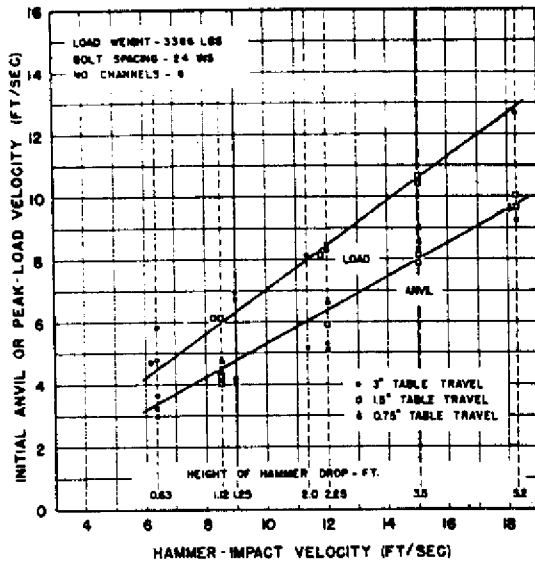


Figure 16 - Initial anvil-table velocity and peak-load velocity - Run 5

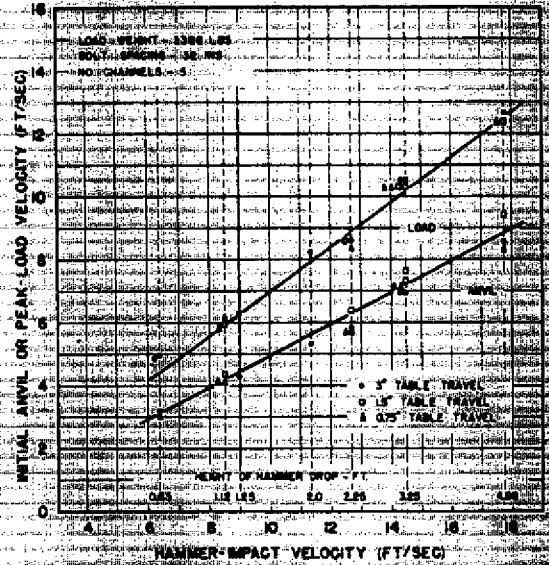


Figure 17 - Initial anvil-table velocity and peak-load velocity - Run 6

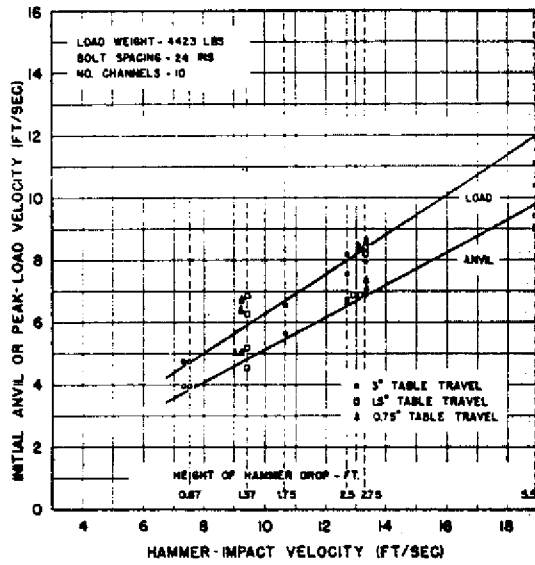


Figure 18 - Initial anvil-table velocity and peak-load velocity - Run 7

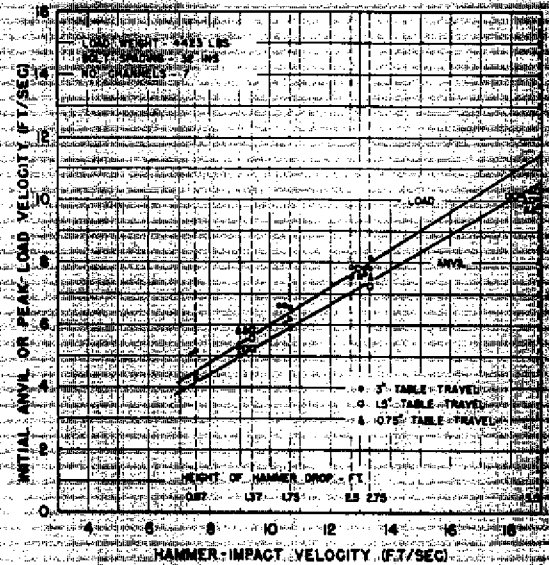


Figure 19 - Initial anvil-table velocity and peak-load velocity - Run 8

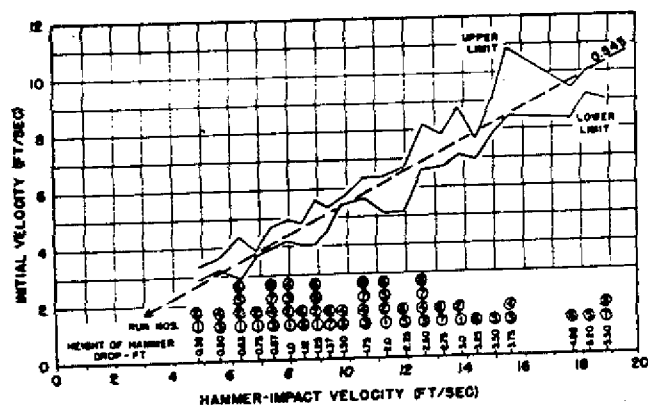


Figure 20 - Initial anvil-table velocity - all runs

Experimental methods comprised (a) determination of average velocity from the nominal anvil-table travel and the time required to reach the upper-limit stops, and (b) a graphical averaging of the anvil-table-velocity curve. The theoretical method was derived by averaging the expression for anvil-table velocity, including gravity, over an integral number of cycles and yielded

$$\bar{v}_2 = \frac{V_0}{1+m} - \frac{1}{2} gT.$$

The experimentally measured value for V_0 was used.

Unfortunately, all three methods are subject to error and produced widely divergent results. The first method is probably the simplest, but requires that the center of the anvil table (instrument location) execute the full amount of travel. This method consistently gave results too large compared to the other methods, often indicating average velocities larger than initial velocities. The graphical integration method suffers from bottoming discontinuities of the velocity meter and zero shift caused by the natural frequency of the seismic element when the integration is carried over an extended period. This method yielded usable results by allowance for the bottoming discontinuities and application of a correction for the meter response. Anvil-table displacement thus obtained from records selected at random were less than the nominal values of 0.75, 1.5, and 3.0 inches. Because abnormally large average velocities are obtained when nominal displacement values are used and because of the previously mentioned off-center hammer blows, it was indicated that the center of the anvil table did not travel the full distance when reversal occurred, but that one side of the retaining ring struck first owing to a tilting of the table. Under static conditions, a maximum tilt of 3.5 degrees was possible before the hold-down bolts jammed in their guides, making the center of the anvil table 0.75 inch lower than the level at the hold-down bolts. This amount is sufficient to bring the results obtained by integration and theory into agreement. The integrated velocity record is considered most accurate. Representative figures for average velocity, computed by the three methods, are given in Table 4. Correlation between the theoretical and integrated average velocities is best for 3-in.-travel blows because damping usually attenuates the reaction component to a negligible amount. These two methods are in error by about 10 percent for 0.75-in. blows, since reversal often takes place during the first half-cycle where the reaction component is extremely large. The agreement between these latter methods indicates that the average anvil-table velocity may be predicted with reasonable accuracy for any height of hammer drop h , mass ratio m , and anvil-table travel. Figure 21 shows the predicted curves for 0.38-in. travel (0.75-in. travel with maximum tilt) and 3-in. travel, together with experimental average velocities. In general, the curves enclose the majority of test points and conform to general trends, although they appear to be too low for high values of $h/(1+m)^2$. Here reversal occurs within the first cycle of reaction oscillation, which invalidates the assumption that this component averages to zero.

TABLE 4
Anvil-Table Displacement and Average Velocity

Run No.	Height Drop (ft)	Displacement* (in.)	T† (ms)	Average Velocity (ft/sec)		Theoretical‡
				s/T	s ² /T	
Nominal 3" Anvil-Table Travel						
1	3.0	2.39	36.0	6.95	5.53	5.54
2	3.0	2.13	35.0	7.15	5.07	5.20
2	3.0	2.42	35.0	7.15	5.75	5.54
4	3.75	2.46	38.0	6.57	5.39	4.99
Nominal 1.5" Anvil-Table Travel						
1	3.0	1.26	18.0	6.95	5.83	6.19
2	1.25	1.23	27.0	4.63	3.79	4.11
3	3.75	1.25	18.5	6.76	5.63	5.90
4	3.75	1.21	18.1	6.90	5.57	5.93
5	5.2	1.10	18.5	6.76	4.95	5.28
Nominal 0.75" Anvil-Table Travel						
1	3.0	0.46	7.2	8.68	5.32	6.00
2	3.0	0.52	7.3	8.55	5.94	6.65
3	3.75	0.54	6.8	9.20	6.61	7.01
4	3.75	0.40	6.2	10.1	5.37	5.55
5	3.5	0.52	10.7	5.84	4.05	5.06

* Integration of anvil-table velocity record with corrections applied.

† Time for table reversal.

‡ Nominal anvil-table travel distance (inches).

$$s = \frac{v_0}{1 + \pi} - \frac{1}{2} gT$$

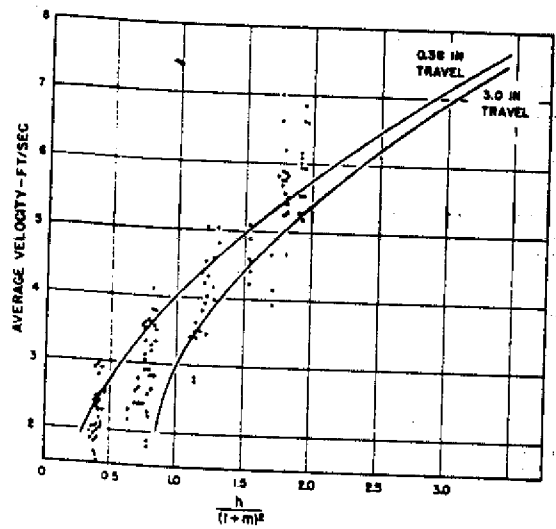


Figure 21 - Predicted average anvil-table velocity for channel-mounted loads

Anvil-Table Reversal Velocity

When the anvil table has risen to its upper limit stops, its motion is suddenly arrested and it rebounds downward with a new velocity which is determined by the coefficient of restitution and the striking velocity. On the test records, reversal is indicated by a step in the anvil-table velocity trace, which is distinguishable from meter-bottoming discontinuities by its sharper break and lesser slope. A sharp peak appears on the anvil-table acceleration trace at the same time. Despite the fact that meter-bottoming discontinuities and the restoring forces on the seismic element make determination of anvil-table velocity at the moment of impact impractical, the reversal step is accurately displayed on the record.

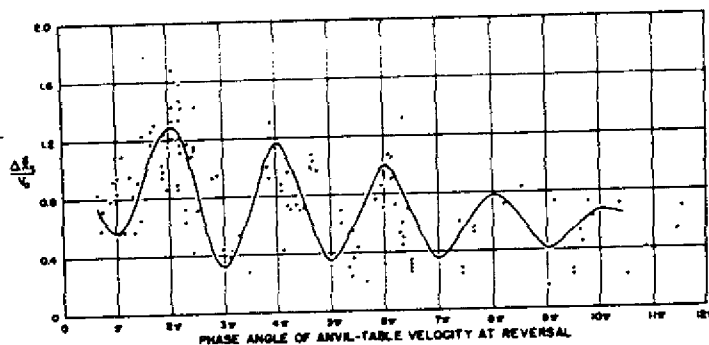


Figure 22 - Variation of anvil-table reversal velocity with phase angle of reaction oscillation

Figure 22 shows the magnitude of the reversal velocity change, relative to initial anvil-table velocity, plotted as a function of the reaction-oscillation phase at reversal. Scatter is quite evident between blows with identical test conditions and between runs on different load weights. On the average, however, points which lie in the vicinity of a whole number of cycles are noticeably larger than those which occur near the alternate half-cycles. This is to be expected, since the anvil table has its greatest velocity at integral cycles after impact and, consequently, should experience the greatest velocity change at these times. The reversal velocity change averages 1.3 times the initial anvil-table velocity in the neighborhood of the first peak and about 1.15 on the second peak. The remaining peaks average unity or less. Figured on a velocity-change basis, the shock is greater for reversal than for initial hammer impact if anvil-table reversal occurs at or near the end of either the first or second cycle of oscillation. The slope of the reversal step is less steep than that caused by hammer impact and alleviates this secondary shock to some extent; these effects will be better borne out by a study of the reversal acceleration. Recognition of the existence of this attribute led to adoption of the two anvil-table travels specified as standard test procedure. If the secondary shock is severe for one distance of table travel, it will probably be proportionally less severe for the alternate travel. Including a series of 0.75-in.-travel blows further reduces the possibility of equipment receiving abnormal secondary shocks for both presently prescribed travel distances. Frequency variations between identical types of equipment of moderately different weight are compensated in this manner, so that neither is inadvertently discriminated against, because the combination of its weight, channel stiffness, and rise time happen to result in a severe secondary shock blow.

Load Velocity - General

The load-velocity waveform, as shown by the typical test records, is nearly sinusoidal in character and exhibits none of the step discontinuities or high-frequency vibrations present on the anvil table, because of the low-pass filter action of the support channels which act as springs. Maximum velocity is reached during the first half-cycle of reaction oscillation; subsequent peaks are attenuated as a result of damping. If the anvil table does not strike its upper limit stops, the load motion decays to a negligible value in 10 to 12 cycles. However, anvil-table reversals impose a new set of transients which may nullify or augment the motions already under way, depending upon their phase when reversal occurs. It is entirely possible for reversal to cause a greater velocity change than that

resulting from hammer impact, which consequently subjects the load to greater shock forces.

Peak-Load Velocity

The peak velocity attained by the load was computed from the amplitude of the first peak, the largest in every case. Data for each of the eight experimental runs were plotted against hammer-impact velocity, together with the initial anvil-table velocity (Figures 12 through 19). Point symbols denote the different anvil-table travels. As with the initial anvil-table velocity, these curves are apparently straight lines passing through the origin and indicating a linear relationship with the hammer-impact velocity. In contrast to the initial anvil-table velocity, however, the slopes of these latter curves varied from 1.08 for the lightest load to 0.60 for the heaviest load; conjugate runs, the same load with different spacing, were nearly the same. Variations in peak-load velocity as a function of the load weight for representative heights of hammer drop are shown in Figure 23. These curves were computed from the slopes of the load-velocity versus

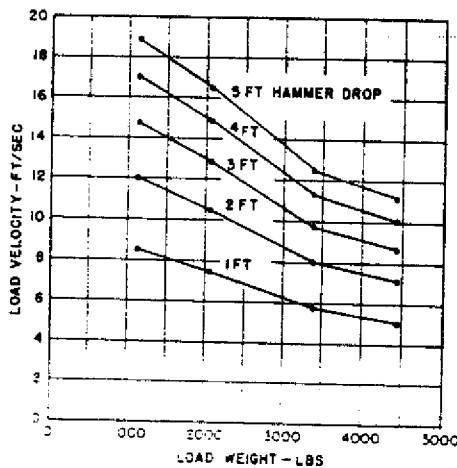


Figure 23 - Peak-load velocity vs. load weight

hammer-impact-velocity curves, since the same heights of hammer drop were seldom employed in more than two runs. Class A tests produced peak-load velocities ranging from 8.3 ft/sec for a Group I blow to 11.5 ft/sec for either a Group II, III, or IV blow, although corresponding groups yielded 6.9 and 9.1 ft/sec load velocities for a Class B test. The above figures are averaged for the eight experimental runs; individual readings varied by approximately 9 percent. In general, heavier loads showed smaller peak velocities.

Load Velocity Resulting From Table Reversal

As a result of anvil-table reversal, the load experiences an additional shock which is added to the motions already under way. If reversal occurs at a time when the load has its maximum velocity on odd half-cycles, the peak velocity, after reversal, may be twice as large as the peak caused by hammer impact. Reversal velocity changes of the load decrease from this

maximum as the phase angle departs from the odd half-cycles and become a minimum on even half-cycles, despite the fact that the anvil-table-reversal step is largest at this point. Figure 11 shows the dependence of load-reversal velocity with phase angle for an ideal case under the conditions stated earlier. In the practical case, damping reduces the amplitude of the oscillating component and consequently causes the maximum reversal velocities to become less as the time to reversal is increased. Figure 24 shows a plot of the ratio of reversal load velocity to initial peak load velocity, plotted as a function of the phase angle at reversal and shows the magnitude of the variations. For reversals which occur at the first load-velocity peak, the velocity change is twice as great as the initial velocity; if it occurs on the load-velocity minimum a half-cycle later, the ratio is only 0.5, a spread of 4 to 1. Successive peak-to-trough ratios become slightly less and are down to approximately 3 to 1 on the fourth cycle. Effects of phasing are clearly shown by this plot and a change of only eight milliseconds ($1/2$ cycle at 65 cps) in rise time may change the load-reversal velocity by a factor of four.

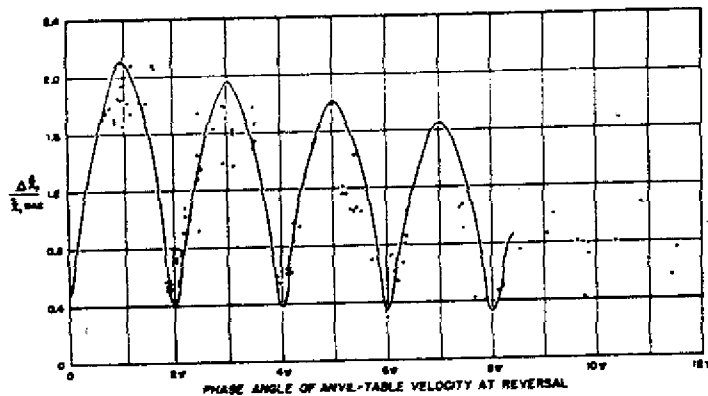


Figure 24 - Variation of load-reversal velocity with phase angle of reaction oscillation

Anvil-Table Acceleration - General

Acceleration signals were passed through either a 300- or 1000-cps low-pass filter before being recorded; the 1000-cps filter was used predominantly. These filters removed accelerometer resonances and the higher vibratory modes on the anvil table which obscure the rigid body motions. The principal frequency present in the 1000-cps-filter records is about 750 cps, and it appears immediately after hammer impact and persists for 3 to 5 cycles. Anvil-table velocity records show the same vibration. Acceleration components of high-frequency are generally not noticeable on the load. Records for the 300-cps filter show a wave form considerably different since the principal frequency of the anvil was outside its passband region. Here, the starting transient has been reduced in amplitude and spread out along its base line, a condition characteristic of a filter excited by pulses whose periods are shorter than the cutoff period.

Peak Anvil-Table Acceleration

The peak anvil-table acceleration occurred immediately after the hammer impact for both the 300- and 1000-cps filter records, although the magnitudes were considerably different. Figures 25 through 32 show these peak measurements plotted against hammer-impact velocity. As with measurements of anvil-table velocity, the curves are straight lines passing through the origin and have essentially the same slope for all eight experimental runs. Figure 33 shows a combined plot of these data for all runs and both filters. Peak accelerations ranged from 220g for the lowest Class B blow of 0.75 ft up to 580g (g = units of gravity) for the maximum height blow of 5.5 ft with a 1000-cps filter. Corresponding measurements, using a 300-cps filter, yielded accelerations in the range of 80 to 200g.

The independence of anvil-table acceleration to weight of channel-mounted load is noted here, as it was for initial anvil-table velocity, and provides a mutual check of instrumentation. Assuming that the initial acceleration is a half-sine pulse, it may then be integrated for the inclosed area and compared to the measured initial anvil-table velocity change. Thus

$$\int_0^{\pi/\omega} \ddot{x}_2 dt = \int_0^{\pi/\omega} \omega^2 x_2 dt = \int_0^{\pi/\omega} a\omega^2 \sin \omega t dt = 2a\omega.$$

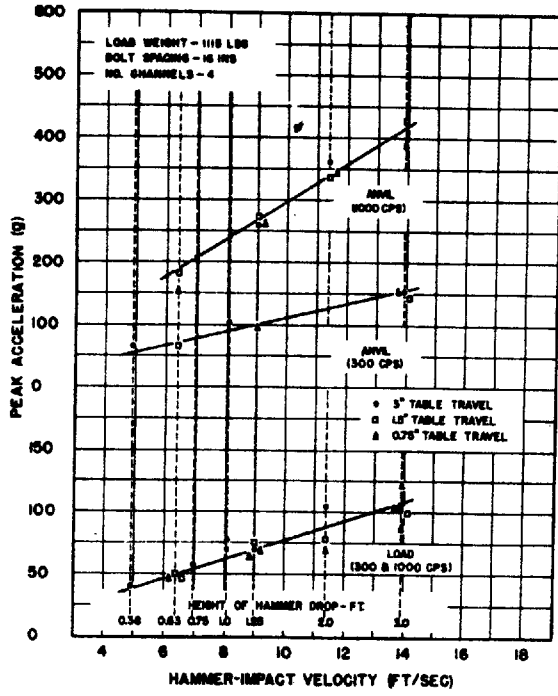


Figure 25 - Peak anvil-table and load acceleration - Run 1

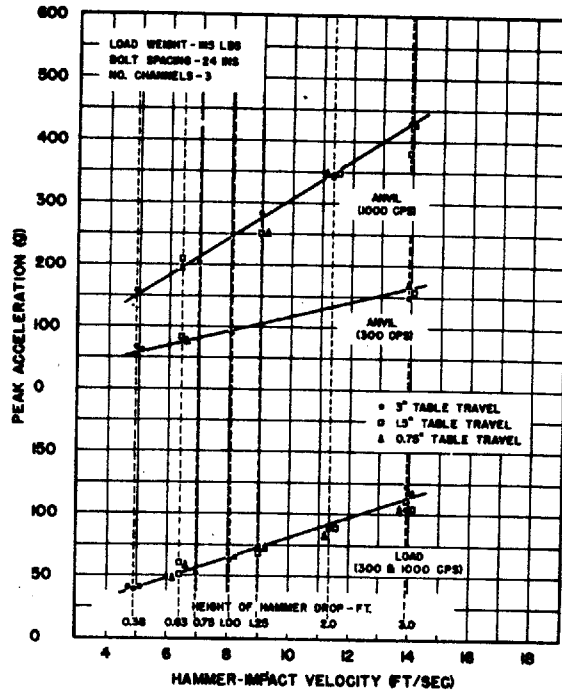


Figure 26 - Peak anvil-table and load acceleration - Run 2

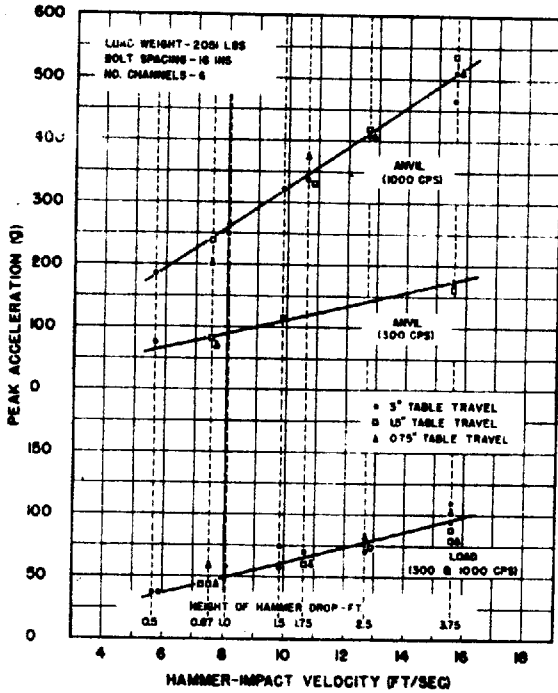


Figure 27 - Peak anvil-table and load acceleration - Run 3

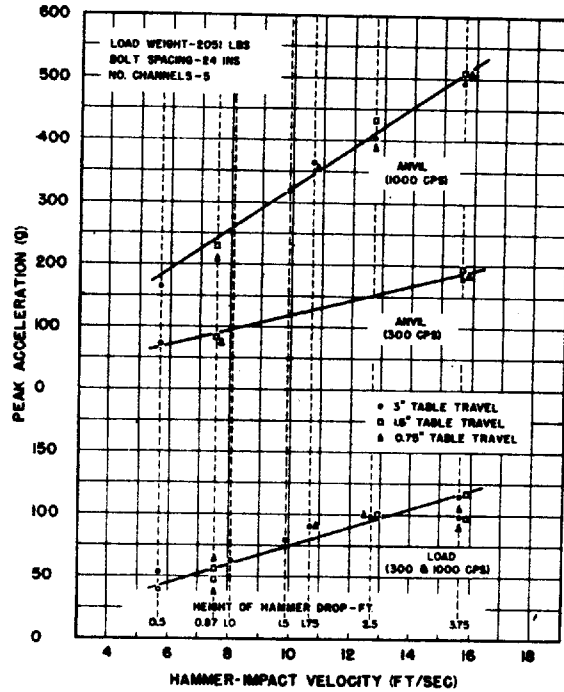


Figure 28 - Peak anvil-table and load acceleration - Run 4

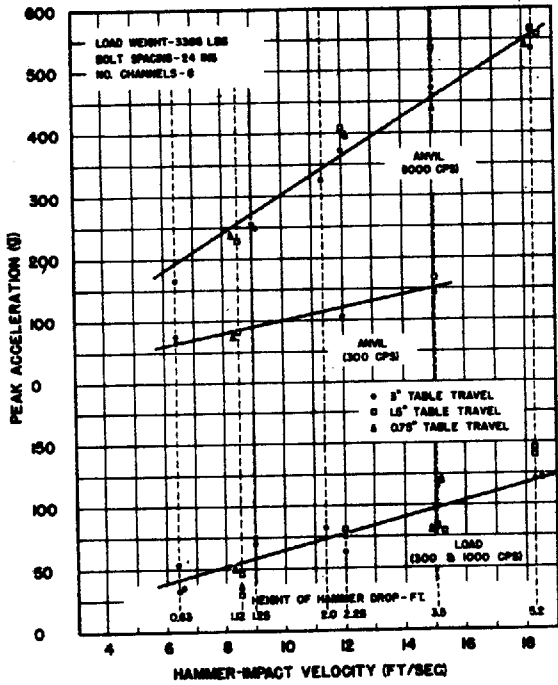


Figure 29 - Peak anvil-table and load acceleration - Run 5

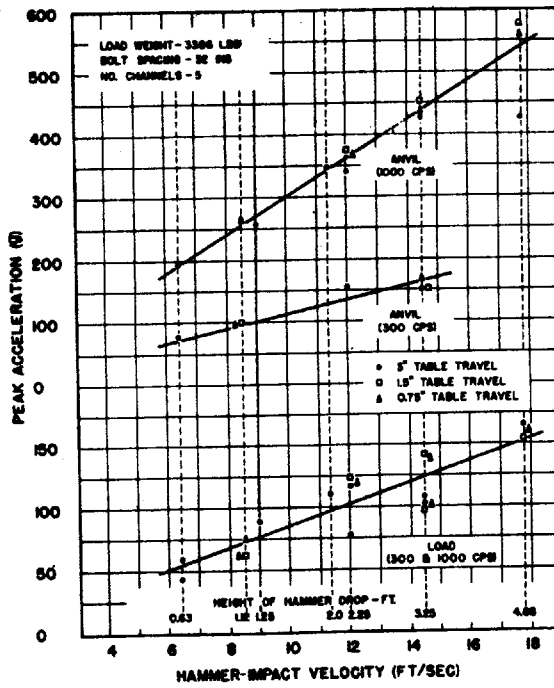


Figure 30 - Peak anvil-table and load acceleration - Run 6

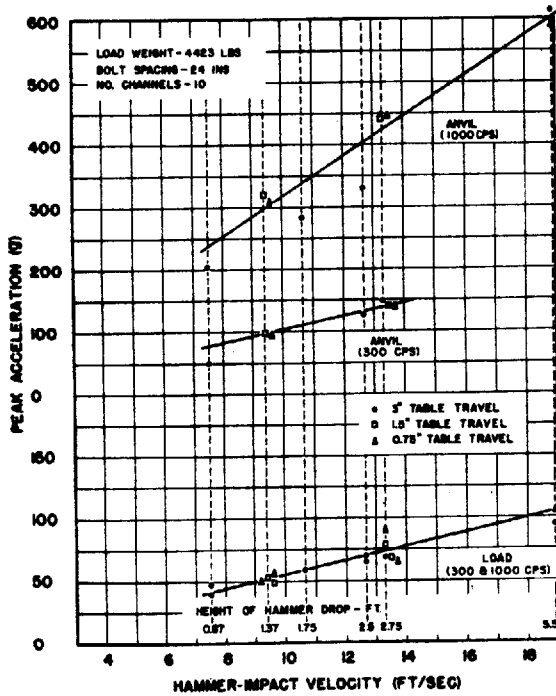


Figure 31 - Peak anvil-table and load acceleration - Run 7

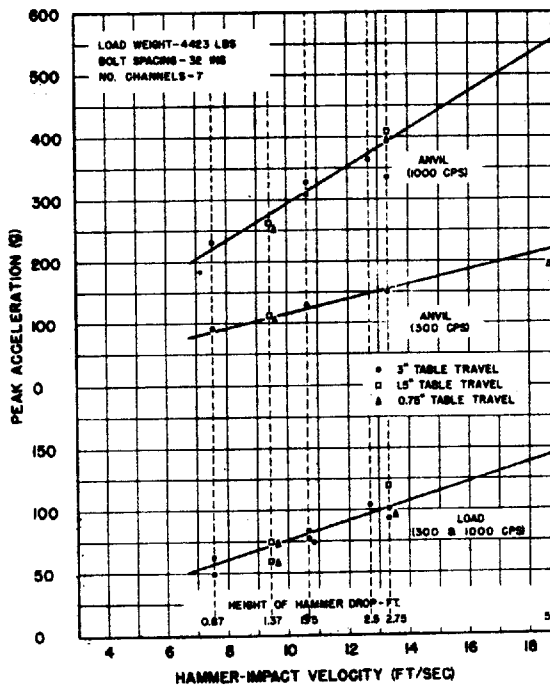


Figure 32 - Peak anvil-table and load acceleration - Run 8

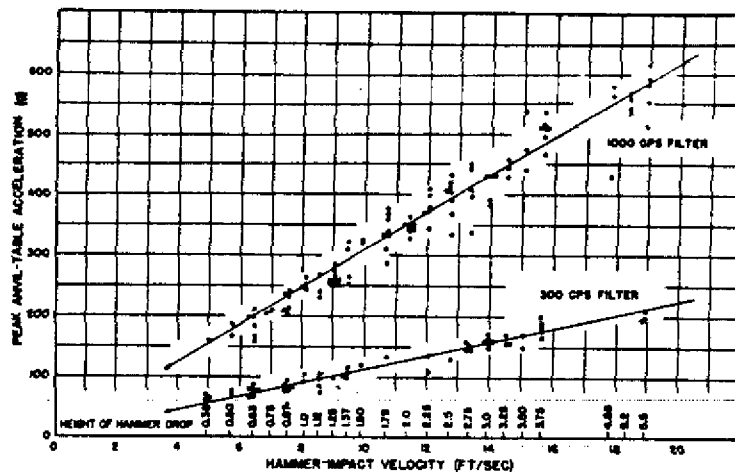


Figure 33 - Peak anvil-table acceleration - all runs

From Figures 20 and 33, initial anvil-table velocity and peak anvil-table acceleration are obtained for any specified height blow; for instance, at 10 ft/sec impact velocity

$$\ddot{x}_2 = 310g \quad \text{and} \quad \dot{x}_2 = 5.4 \text{ ft/sec.}$$

Using this acceleration value, the computed velocity becomes

$$\dot{x}_2 \Big|_{t = \pi/\omega} = 2a\omega = 4.24 \text{ ft/sec,}$$

which is of the same order of magnitude as the measured value of 5.4 ft/sec. If allowance is made for the filter-transmission characteristic (70 percent at 750 cps), a calculated value for anvil-table velocity of 6.05 ft/sec is obtained. This is in good agreement with the value obtained.

Anvil-Table Reversal Acceleration

A negative acceleration pulse appears on the anvil-table acceleration trace as a result of its impact with the upper limit stops. In general, the reversal acceleration is a single pulse as contrasted to the damped vibration of the initial acceleration; i. e., no table vibratory modes are excited to any measurable extent. Differences between response to these two impact types may be attributed to the different mechanisms involved in starting and stopping the anvil table. Stopping forces are taken by the limit ring and table bolts and are spread out over a considerably longer time than hammer impacts. Tilting of the anvil table probably contributes, since the few bolts which first take the strain are more resilient than a direct hammer-anvil collision.

Phase angle of the reaction oscillation at table reversal is relatively unimportant in this instance because the amplitude of the reaction component is small compared to the starting peak acceleration. The reversal acceleration depends mostly on the magnitude of the velocity change and the time required to execute it. Although the velocity change was shown to be dependent on phase angle, the time element is affected by the resilience of the stopping bolts, an extremely random event because of the tilt at the time of reversal. Anvil-table reversal usually requires 2 to 4 milliseconds; Figure 34 shows the ratio of reversal to peak acceleration plotted against phase angle. Except for the one series of higher than average values near the first cycle, the points indicate considerable scatter throughout the entire range with no pronounced trends attributable to phase angle. On the average, the ratio of reversal to peak acceleration drops from 0.6 during the first cycle to approximately 0.3 for the fifth.

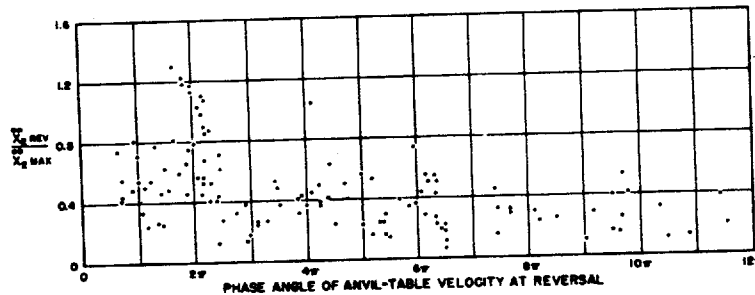


Figure 34 - Variation of anvil-table reversal velocity with phase angle of reaction oscillation

Load Acceleration - General

Both the 300-cps and 1000-cps low-pass filters were employed in the circuit recording load accelerations, although the percentage of higher order frequencies was almost negligibly small because of isolation afforded by the support channels. Consequently, load-acceleration waveforms obtained by either filter are nearly identical, and for the lighter loads and hammer blows they are approximately sinusoidal. As the load and hammer height are increased, amplitude distortion becomes more noticeable owing to nonlinearities in the support channels. These manifest themselves as a change in frequency between positive and negative halves of one cycle of reaction oscillation, positive peaks occurring at a higher frequency and possessing a larger amplitude than negative peaks.

Peak-Load Acceleration

The peak acceleration caused by hammer impact occurs during the first half-cycle of oscillation; peaks which follow, except for reversal, are attenuated by damping. Plots of peak-load acceleration are included in Figures 25 through 32. A single curve denotes the results obtained with both filters. It is observed again that peak-load accelerations are linearly related to the hammer-impact velocity and are somewhat dependent on load and bolt spacing. Table 5 presents a summary of the peak-load accelerations measured for the maximum and minimum height blows specified for both Class A and B tests.

Peak-load accelerations ranged between 60g and 96g for the minimum height and between 78g and 144g for the maximum height blows scheduled for Class A tests. Higher

accelerations were associated with the heavier load weights. Class B tests showed peak accelerations averaging about 80 percent as large as Class A blows.

TABLE 5
Load Acceleration for Class A and B Tests (300- or 1000-cps low-pass filters)

Run No.	Bolt Spacing (in.)	Peak-Load Acceleration (units of gravity)			
		Class A		Class B	
		Group I	Groups II, III, and IV	Group I	Groups II, III, and IV
1	16	63	85	54	70
2	24	66	92	57	73
3	16	60	78	49	65
4	24	73	95	60	80
5	24	74	98	58	79
6	32	96	124	77	102
7	24	70	104	59	73
8	32	96	144	81	102

Figure 35 shows the range of load acceleration caused by hammer impact, possibly expected for a Class A test using the three bolt-spacing dimensions employed in this investigation. The 24-inch spacing was the only one for which data were obtained for all loads, and this fact indicates that, if the specified number of support channels are used, peak-load accelerations remain relatively independent of load weight. For the same load weight, but with a different number of channels, the 32-inch spacing yields somewhat larger load accelerations and the 16-inch spacing produces lesser accelerations.

Load Acceleration after Table Reversal

When the anvil table reverses, the phase of reaction oscillation is relatively important, and could cause velocity changes on the load which are larger than those attributed to initial hammer impact. Since the acceleration of the load is essentially the differentiation of the principal frequency occurring in the velocity record, effects of table reversal will be similar. Figure 36 shows how the phase angle affects the load-acceleration magnitude after table reversal. Peaks are centered around the integral half-cycles and reach values (ratio of acceleration to initial peak-load acceleration) averaging about 1.2 for the first half-cycle and 1.0 or less after the third half-cycle. A minimum of about 0.2 occurs on the whole cycles.

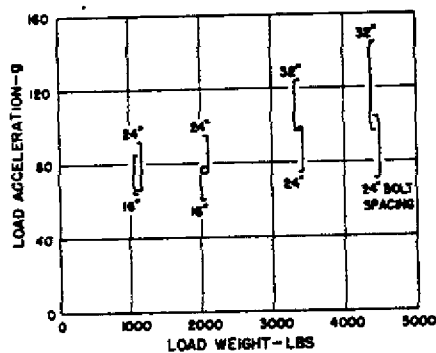


Figure 35 - Load acceleration range for Class A tests

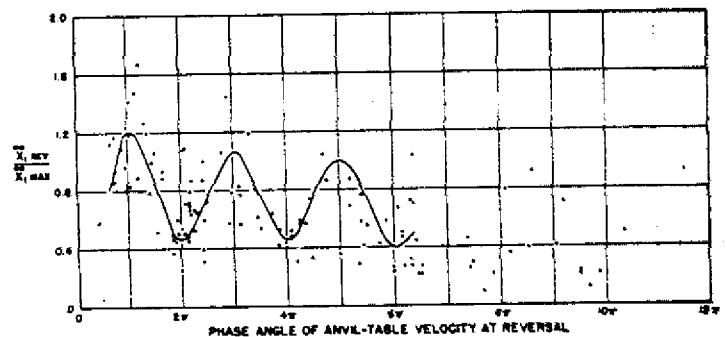


Figure 36 - Variation of load-reversal acceleration with phase angle of reaction oscillation

Load Frequency

For the lighter loads and lower hammer drops, the waveforms of velocity and acceleration on both the anvil table and load are nearly sinusoidal. However, as the load and/or hammer drop are increased, the waveforms become progressively more distorted, and the frequency gradually decreases as the load motion becomes less violent. Frequency variations and waveshape distortion can be attributed to nonlinearities and to a direction sensitivity in the support channels. The latter is caused by a change in end conditions with direction of deflection. When the support channels are being deflected toward the anvil table (positive load acceleration), they deflect beyond the inner edges of the base channels; for deflection away from the anvil table they pivot around the outer edges of the base channels. Besides a shortening of effective length with downward deflection, end conditions change from a hinge-type pivot to a clamped-end condition, which is considerably stiffer. In determining the load-reaction frequency, at least three and preferably four cycles were included in the count. Frequencies listed for each run are then the average of all frequency measurements for a given run and represent the most probable value which can be assigned to this quantity (Table 6).

TABLE 6
Average Reaction Frequency

Run No.	Number of Channels	Bolt Spacing (in.)	Load Weight (lb)	Average Frequency (cps)
1	4	16	1115	65.6
2	3	24	1115	71.4
3	6	16	2051	55.4
4	5	24	2051	57.5
5	8	24	3386	65.5
6	5	32	3386	68.1
7	10	24	4423	70.6
3	7	32	4423	67.7

Reed-Gage Data

Reed-gage records have been analyzed and an additional report will be prepared and submitted in the near future.

Correlation between Theoretical and Experimental Results

The waveforms obtained experimentally are in good agreement with the idealized curves of Figure 10 when allowances are made for gravity effects and errors introduced over extended periods of time by the velocity-meter seismic element. The shock delivered to the anvil table can then be adequately described as an impulsive type, characterized by a step-velocity change. Correlation was good between experimental and theoretical methods of computing average anvil-table velocity. A second example is given in Table 7 by comparing mass ratio with dead-weight measurements and from the experimental data. If damping is neglected during the first half-cycle of reaction oscillation, the maximum and minimum anvil velocity evaluated from the expression derived in Appendix II becomes

$$\dot{x}_2 \max \Big|_{t=0} = V_0 \qquad \dot{x}_2 \min \Big|_{t=\pi/\omega} = V_0 \left[\frac{1-m}{1+m} \right]$$

from which

$$m = \frac{\dot{x}_2 \max - \dot{x}_2 \min}{\dot{x}_2 \max + \dot{x}_2 \min}$$

In determining the weights which make up either mass, one half the weight of the supporting channels was added to the load and one half to the table.

TABLE 7
Comparison of Mass Ratio

Run No.	Total Load Wt (lb)	Anvil-Table Wt (lb)	Calculated Mass Ratio	Experimental Mass Ratio
1	1265	5093	0.25	0.26
2	1223	5058	0.24	0.25
3	2358	5168	0.46	0.53
4	2320	5130	0.45	0.49
5	3686	5143	0.70	0.73
6	3573	5130	0.70	0.73
7	4798	5318	0.90	0.89
8	4686	5206	0.90	0.83

Figures given as experimental data were the average of the twenty-odd blows struck during each of the test runs; individual figures varied by as much as 10 percent from the average. Techniques employed in determining the minimum velocity follow those mentioned earlier as an average line was drawn through the anvil-table vibrations.

Correlation between theory and experiment for load velocities is not as good as might be expected, because nonlinearities and direction sensitivities in the supporting channels are not accounted for in the theoretical treatment. In addition, no allowance was made for components owing to the initial static-channel deflection. Thus the peak theoretical load velocity is

$$\frac{\dot{x}_1 \max}{V_0} = \frac{2}{1+m}$$

when gravity and damping are omitted. Table 8 gives the correlation between methods and indicates that the experimental data consistently ran higher than computed figures; the difference is greatest for the lighter loads, decreasing with an increase in mass ratio. In a similar manner, the peak load acceleration may be computed as

$$\frac{\ddot{x}_1 \max}{V_0 \omega} = \frac{\omega}{1+m}$$

Here, the error between results (Table 8) is considerably greater, as might be expected, for a higher order function.

TABLE 8
Comparison of Experimental and Theoretical Results

Run No.	Mass Ratio	Frequency (cps)	Peak Load Velocity			Peak Load Acceleration		
			$\frac{x_1 \text{ max}}{V_0}$	$\frac{2}{1+m}$	Per- cent Error	$\frac{x_1 \text{ max}}{V_0}$	$\frac{\omega}{1+m}$	Per- cent Error
			Experimental	Theoretical		Experimental	Theoretical	
1	0.25	65.6	1.91	1.60	16.2	14.4	10.2	29.2
2	0.24	71.4	2.00	1.61	19.5	15.0	11.2	25.3
3	0.46	55.4	1.67	1.37	17.6	11.5	7.4	35.7
4	0.45	57.5	1.74	1.38	20.3	13.9	7.7	44.6
5	0.70	65.5	1.30	1.17	10.0	12.0	7.5	37.4
6	0.70	68.1	1.30	1.17	10.0	15.7	7.8	50.3
7	0.90	70.6	1.17	1.05	10.3	10.4	7.2	30.8
8	0.90	67.7	1.11	1.05	5.4	14.3	7.0	57.0

As can be seen from the foregoing discussions, channel stiffness plays an extremely important part in the determination of peak-load accelerations. With the instrumentation used during this investigation, channel stiffness was not a directly measurable quantity, but two methods are available for evaluating it indirectly from the recorded data. Method I makes use of the expression derived in Appendix II for frequency of oscillation, which, when rearranged, becomes

$$k = \frac{M_1 M_2}{M_1 + M_2} \omega^2,$$

and Method II utilizes the measurement of peak positive load acceleration in the expression

$$\sqrt{k} = \frac{\sqrt{g_1(1-\pi)}}{V_0} x_1 \text{ max.}$$

Table 9 lists channel-stiffness values computed by both methods.

TABLE 9
Computed Values for Channel Stiffness

Run No.	No. of Channels	Bolt Spacing (in.)	Frequency (cps)	Stiffness (10^6 lb/ft/channel)	
				Method I	Method II
1	4	16	65.6	1.34	2.59
2	3	24	71.4	2.05	3.72
3	6	16	55.4	1.01	2.35
4	5	24	57.5	1.29	4.06
5	8	24	65.5	1.42	3.65
6	5	32	68.1	2.30	9.88
7	10	24	70.6	1.54	2.94
8	7	32	67.7	1.98	8.10

A plot of these data against load-bolt spacing is given in Figure 37, together with the calculated stiffness of a simple-ended beam. In general, Method I yields stiffnesses which are less than the calculated stiffness of the simple beam, but Method II data are all greater.

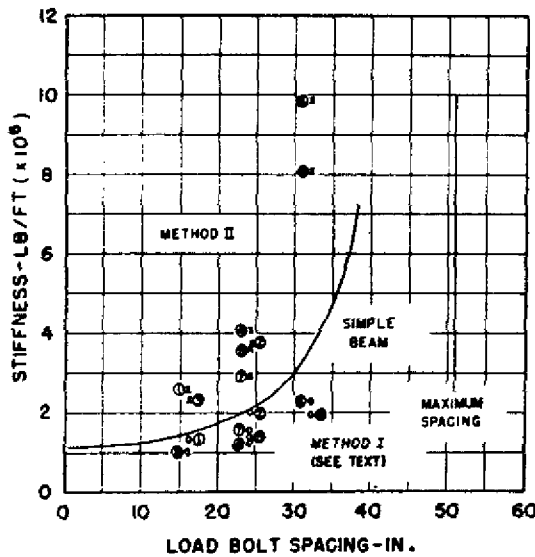


Figure 37 - Computed channel stiffness

weight. This study was made to ascertain the magnitude, frequencies, and general characteristics of the shock delivered by this machine under standard operating conditions. Data taken are then compared with shock data obtained aboard ship under actual combat conditions and will serve as a basis for comparing the performance of other shock machines of similar type.

Dead-weight loads, ranging throughout the capacity of the machine, were mounted according to specifications and subjected to a series of blows corresponding to the magnitudes given Class A and B equipments. In addition to the standard test procedure, blows equivalent to 50 percent of Class B and 150 percent of Class A blows were delivered, and a third table-travel distance of 0.75 inch was included.

Measurements were made on the load and at the center of the anvil table by two groups of instruments, each group including an accelerometer, a velocity meter, and a multifrequency reed gage. Output signals were recorded as a function of time by standard cathode-ray-oscillographic techniques and simultaneously by a multichannel Mirragraph system.

Peak values of initial anvil-table velocity and table acceleration are linearly related to hammer-impact velocity and are independent of the weight of the channel-mounted load. Values ranging up to 10.3 ft/sec and 580g, (1000-cps filter) were measured on the anvil table for the maximum hammer drop of 5.5 ft. Two principal frequencies were encountered on the anvil table—a 750-cps component caused by elastic vibrations in the table excited by the hammer blow and a lower frequency of approximately 65 cps attributed to the reaction of the relatively flexibly mounted load. Peak values of load velocity and acceleration are also linearly related to hammer-impact velocity, but are dependent

The coefficient of critical damping varies widely between consecutive peaks of the same blow and between identical hammer blows. In general, it becomes larger as the amplitude decreases; this indicates a larger percentage of friction damping. The methods of securing the load on the Medium-Weight Shock Machine in specification shock tests make it likely that damping in the order of 4 to 5 percent of critical may be expected.

SUMMARY

The Medium-Weight Shock Machine has been used since 1943 to determine the resistance of naval shipboard equipment to shock damage. Units to be shock tested are secured to standard mounting adapters to simulate the stiffness of their foundations aboard ship and are then subjected to a series of shock blows, the magnitude of which is governed principally by their

on load weight. Maximum values which might be expected for a typical Class A test are 11.5 ft/sec for velocity and between 80g and 144g for acceleration, becoming larger for the heavier loads. The principal frequency averaged around 65 cps.

It is shown mathematically that the anvil table and its load could be approximated to a fair degree of accuracy by a single-degree-of-freedom system of two-coupled masses. On the basis of these derived equations, representative values of mass ratio, damping, and channel stiffness were computed.

ACKNOWLEDGMENTS

The author wishes to express his obligation to Mr. F. J. Bury and Mr. R. J. Peters for their assistance with this project and to Mr. J. P. Walsh and Dr. I. Vigness for their many helpful suggestions in the preparation of material for this report.

REFERENCES

- (1) Conrad, R. W., "Characteristics of the 250 Ft-lb Shock Machine, ' NRL Report F-3328 (Unclassified), July 1948.
- (2) Conrad, R. W., "Characteristics of the 3 Ft-lb Vibration Machine," NRL Report S-3186 (Unclassified), October 1947.
- (3) Vigness, I., "Mechanical Shock Characteristics of the Armour High-Impact Machine for Electronic Devices " (Armour Research Foundations Machine No. 1), NRL Report O-2485 (Unclassified), March 1945.
- (4) Vigness, I., Kammer, E. W., and Holt, S., "Mechanical Shock Characteristics of the High-Impact Machine for Electronic Devices " (NRL Machine No. 1), NRL Report O-2497 (Unclassified), March 1945.
- (5) Vigness, I., Nowak, R. C., and Kammer E. W., "Mechanical Shock Characteristics of High-Impact Machines for Electronic Devices submitted by Taft-Peirce Co.," NRL Report O-2838 (Unclassified), December 1946.
- (6) Kirkpatrick, T. P., "Medium-Weight High-Impact Shock Machine Characteristics ' Symposium on Shock, Vol. II, p. 48, BuShips, 30 October 1943.
- (7) Young, S. E., "Effect of Modifications on the Performance Characteristics of the Light-Weight, High-Impact Shock Machine," NRL Report V-2666 (Unclassified), October 1945.
- (8) Lorraine, R. G., "Light-Weight Class H. I. Shock Machine Characteristics," Symposium on Shock, Vol. II, BuShips, 30 October 1943.
- (9) BuShips Specification 40T9 (Ships) dated 15 December 1946.
- (10) Military Specification MIL-S-901 (Ships) dated 15 November 1949.
- (11) NRL Ltr. Report 3850-328A/50, RWC:mlhb dated 15 September 1950.
- (12) NRL Ltr. Report 3850-56/51, RWC:mlhb dated 22 March 1951.
- (13) Walsh, J. P., and Blake, R. E., "The Determination of Shock Isolation Performance," NRL Report F-3596 (Unclassified), 6 January 1950.

APPENDIX I

Descriptive Details of Mounting Arrangements

The following comments on the methods used in arranging the support channels for this investigation are not intended to imply that these methods are preferred. Detailed drawings of the load apparatus are shown in Figures 38 through 41.

Run 1 - Four car-building channels were required, one pair of which was located along each load-bolt line. The load feet rested on 7 in. x 9 in. x 1 in. steel plates which spanned both channels of a pair.

Run 2 - Three car-building channels were required. One pair, consisting of one standard and one car-building channel, was located along each load-bolt line. The load feet rested on 7 in. x 9 in. x 1 in. steel pads (Figure 4).

Run 3 - Six car-building channels were required. Two pairs of channels, each consisting of one car-building and one standard channel, were arranged along each bolt line. The load feet rested at the center of 8 in. x 14 in. x 1 in. steel plates which spanned the two pairs of channels. Distance between the center lines of pairs of channels along one bolt line was 8-3/4 inches.

Run 4 - Five car-building channels were required. One pair of channels, consisting of one car-building and one standard channel, and a second pair of channels, comprising two standard channels, were located along each load-bolt line. As before, the center spacing between adjacent pairs of channels was 8-3/4 inches, and the load rested on 8 in. x 14 in. x 1 in. steel pads which spanned the two pairs. The channel pair comprising the two standard channels was placed inboard of the bolt line.

Run 5 - Eight car-building channels were required. Four pairs were located at approximately equal intervals along the entire length of the base channels. Across the top and at right angles to these, were bolted two pairs of 6 in. x 15.6 lb auxiliary channels. Rough-cut 1/2- and 5/8-in.-thick steel plates welded to the upper flanges maintained the spacing between channel members and served as pads for the load feet and connecting bolts. Spacers were also welded into the ends of these channels.

Run 6 - Five car-building channels were required. A total of three pairs of channels were used. One pair of car-building channels was placed under the center of the load. The remaining two pairs, each composed of one standard and one car-building channel, were positioned outboard to yield a support-channel spacing of approximately 21 inches. The auxiliary channels were again used to mount the load. However, to minimize the time for changes in the test setup required by the different bolt spacing, the load was mounted off-center with respect to the auxiliary channels and utilized some of the previously located pads. Only four additional plates which could be installed without disturbing any of the existing plates, were welded to the flanges; two for the load feet and two for the center pair of supporting channels. The slight unbalance caused by the asymmetry of the auxiliary channels was compensated by shifting the load.

Run 7 - Ten car-building channels were required. Chronologically this run was made immediately following Run 5 to minimize dismantling. The four pairs of channels used

in this former run were kept intact in their previous positions; two pairs of channels comprising two standard channels each were installed under the center of the load. Additional attachment plates were welded to the upper flange of the auxiliary channels to secure them. Car-building channels would have been preferred for the additional channels, but they were not available.

Run 8 - Seven car-building channels were required. The off-center arrangement of the auxiliary channels used during Run 6 was employed again here. Two pairs of car-building channels and two pairs, consisting of one car-building and one standard channel, were located under the auxiliary channels with approximately equal spacing. The pairs containing the standard channels were placed outboard.

* * *

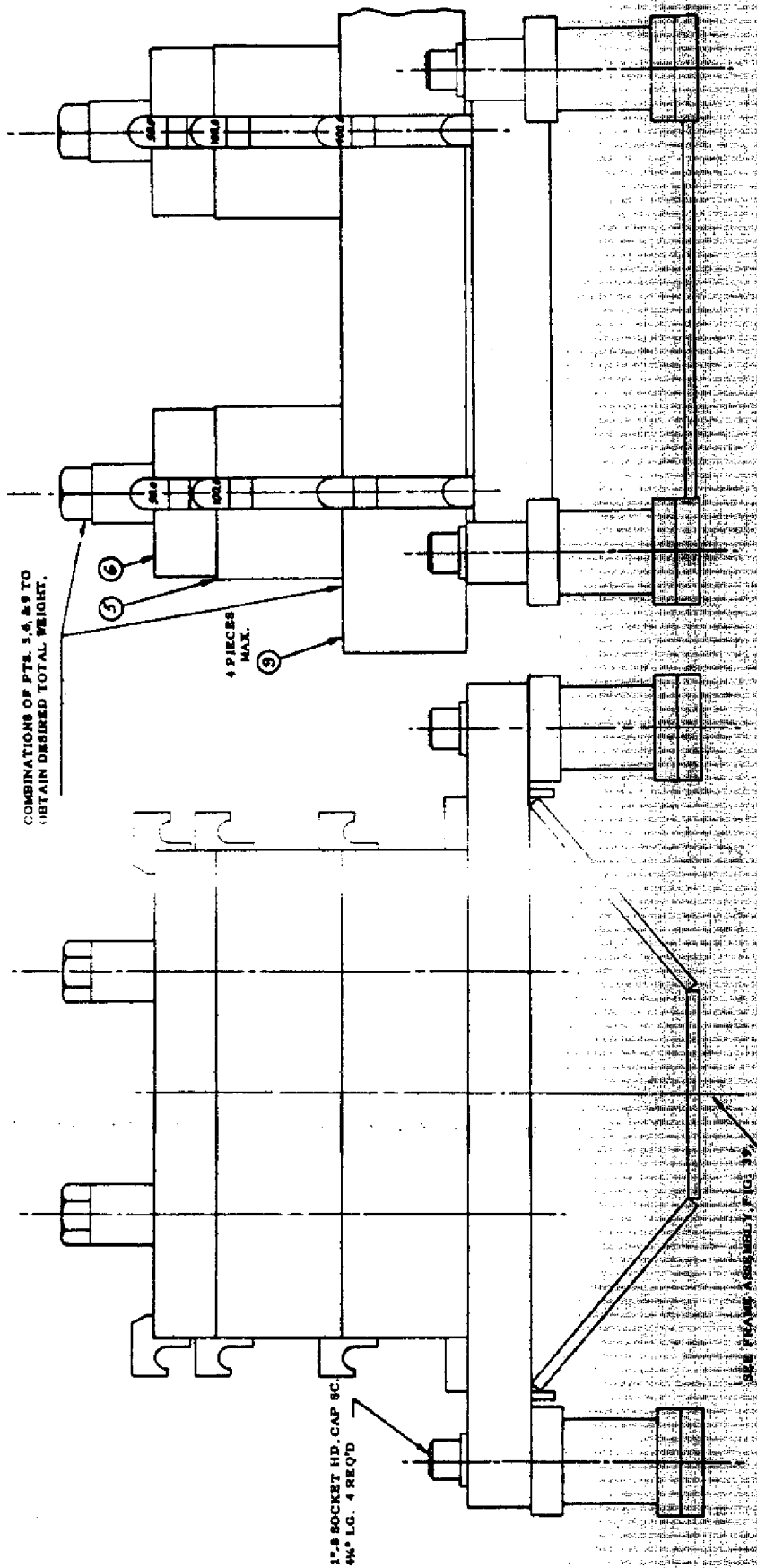


Figure 38 - 1000 lb. apparatus - assembly (200-2000 lb load weight)

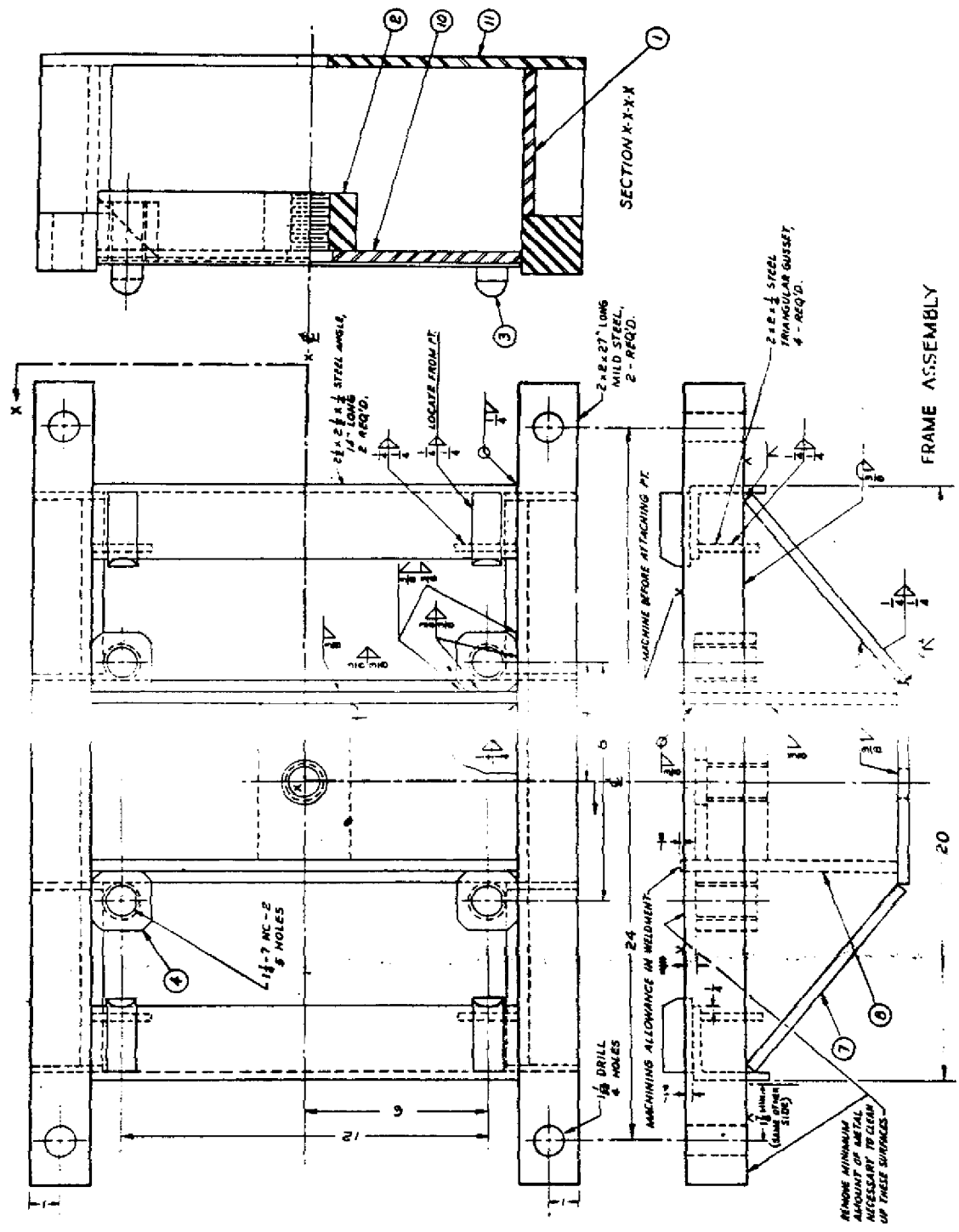


Figure 39 - Load apparatus - light-weight base

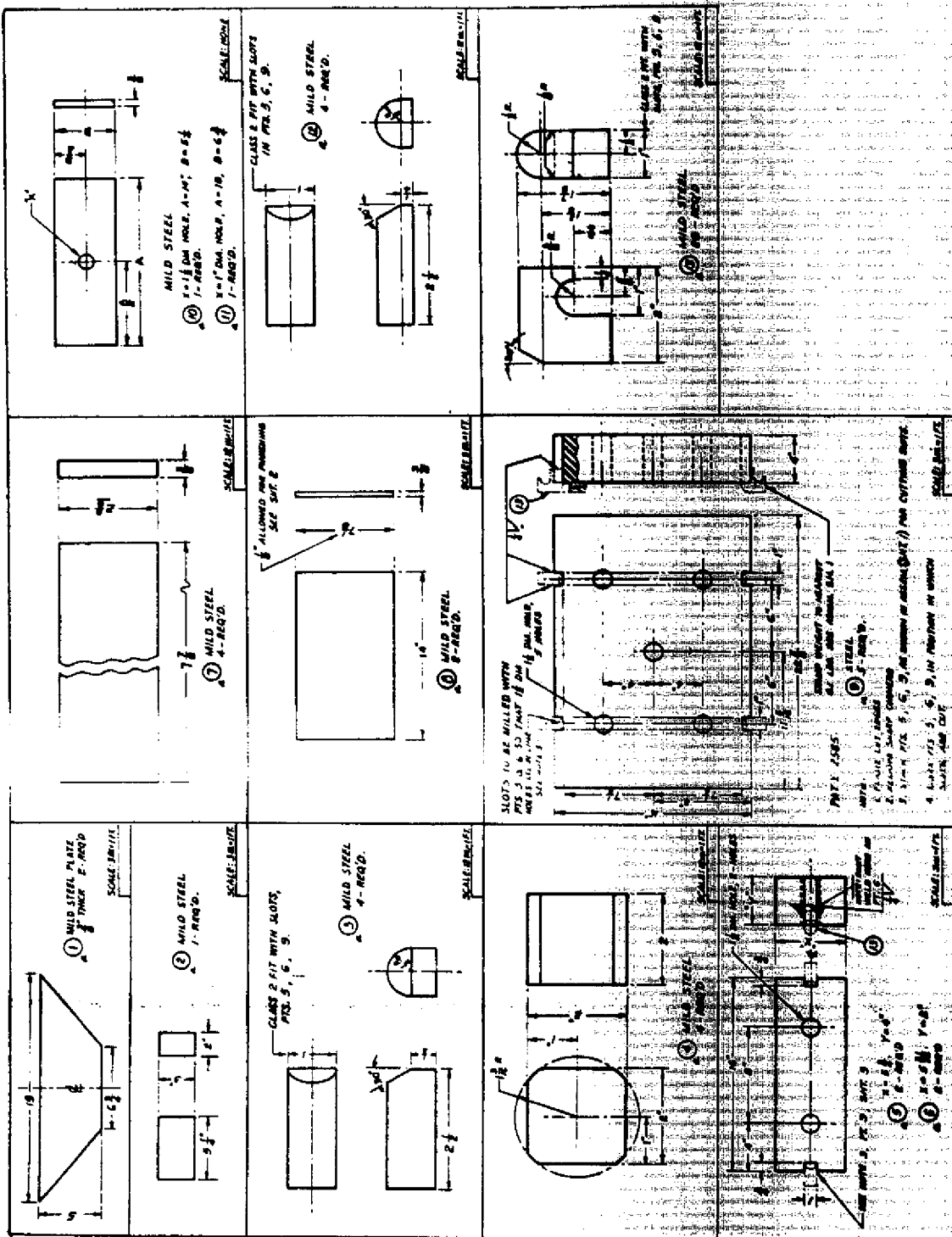


Figure 40 Load apparatus - component parts

APPENDIX II

Derivation of Equations of Motion

The equations of motion for a single-degree-of-freedom system of two coupled masses with viscous damping are derived from the force equations. The force equations for this system are given by

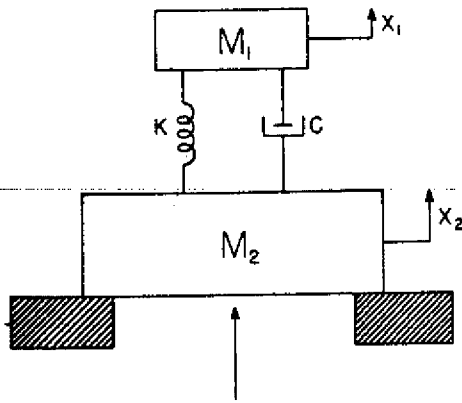


Figure 42 - Equivalent single-degree-of-freedom system

$$-k(x_2 - x_1) - c(\dot{x}_2 - \dot{x}_1) = M_1 \ddot{x}_2 \quad (1)$$

and

$$k(x_2 - x_1) + c(\dot{x}_2 - \dot{x}_1) = M_1 \ddot{x}_1 \quad (2)$$

where \$k\$ is the spring constant, assumed linear, and \$c\$ is the damping coefficient. These equations are second degree, simultaneous differential equations with constant coefficients. Assumptions are made that (a) the spring is linear and massless, (b) damping is viscous, and (c) the effects of gravity can be neglected. Boundary conditions are chosen so that the entire system is at rest prior to \$t = 0\$ and at \$t = 0\$ the lower mass suddenly acquires a velocity \$V_0\$. Expressed mathematically these become

$$\begin{aligned} x_1 = \dot{x}_1 = \ddot{x}_1 = x_2 = 0 \\ \dot{x}_2 = V_0 \end{aligned} \quad \Big| \quad t = 0$$

Resorting to the Laplace Transformation and substituting in the boundary conditions, these equations become

$$(M_2 p^2 + cp + k) \bar{x}_2 - (cp + k) \bar{x}_1 = M_2 V_0 \quad (3)$$

$$(cp + k) \bar{x}_2 - (M_1 p^2 + cp + k) \bar{x}_1 = 0 \quad (4)$$

Solving this pair of simultaneous equations for \$\bar{x}_1\$ yields

$$\bar{x}_1 = \frac{M_2 V_0}{v} \left[\frac{1}{p^2} - \frac{1}{p^2 + \frac{cv}{\mu}} \frac{1}{p + \frac{kv}{\mu}} \right] \quad (5)$$

where $\mu = M_1 M_2$ and $\nu = M_1 + M_2$.

The nature of the solution for the inverse transformation depends upon the form of the roots of the quadratic in the denominator, i. e., the relative values of $\frac{c^2 \nu^2}{\mu^2}$ and $4 \frac{k\nu}{\mu}$. When $\frac{c^2 \nu^2}{\mu^2} = 4 \frac{k\nu}{\mu}$, the case for critical damping, the resulting motion of M_1 is nonoscillatory and reaches its final value in a minimum of time. For $\frac{c^2 \nu^2}{\mu^2} > 4 \frac{k\nu}{\mu}$, the roots are real, and the motion remains nonoscillatory, although the final value is reached at a somewhat later time. This is the overdamped case. The remaining solution is of interest to this problem and occurs when $\frac{c^2 \nu^2}{\mu^2} < 4 \frac{k\nu}{\mu}$, yielding imaginary roots to the operational quadratic. In this event, the motion is oscillatory around its final value, decaying in an exponential manner as determined by the percent of critical damping. The expression for \bar{x}_1 then becomes

$$\bar{x}_1 = \frac{M_2 V_0}{\nu} \left[\frac{1}{p^2} - \frac{1}{(p + \gamma)^2 + \delta^2} \right],$$

where $\gamma = \frac{c\nu}{2\mu}$ and

$$\delta = \frac{1}{2} \left(\frac{4k\nu}{\mu} - \frac{c^2 \nu^2}{\mu^2} \right)^{\frac{1}{2}}. \quad (6)$$

The inverse transformation \bar{x}_1 is then

$$x_1 = \frac{M_2 V_0}{\nu} \left[t - \frac{1}{\delta} (\sin \delta t) e^{-\gamma t} \right]. \quad (7)$$

In this form the expression for the load displacement is obscure and difficult to interpret.

By expressing the damping as a percentage of the critical damping, $\zeta = \frac{c}{c_c}$, the

interrelation of the components is more clearly seen.

$$x_1 = \frac{V_0}{1+m} \left[t - \frac{e^{-\frac{c}{c_c} \omega t}}{\omega \sqrt{1 - \frac{c^2}{c_c^2}}} \sin \omega \sqrt{1 - \frac{c^2}{c_c^2}} t \right] \quad (8)$$

where $m = M_1/M_2$ and $\omega = \sqrt{\frac{k\nu}{\mu}}$.

For small percentages of damping, c/c_c less than 10% for instance, $1 - c^2/c_c^2$ is approximately unity, and for all practical purposes the load displacement becomes

$$x_1 = \frac{V_0}{1+m} \left[t - \frac{e^{-\frac{c}{c_c} \omega t}}{\omega} \sin \omega t \right]. \quad (9)$$

Successive differentiation yields expressions for the load velocity and acceleration given by

$$\dot{x}_1 = \frac{V_0}{1+m} \left[1 + e^{-\frac{c}{c_c} \omega t} \left(\frac{c}{c_c} \sin \omega t - \cos \omega t \right) \right] \quad \text{and} \quad (10)$$

$$\ddot{x}_1 = \frac{V_0 \omega}{1+m} \left[\left(1 - \frac{c^2}{c_c^2} \right) \sin \omega t + 2 \frac{c}{c_c} \cos \omega t \right] \quad (11)$$

These simplify to

$$\dot{x}_1 = \frac{V_0}{1+m} \left[1 - e^{-\frac{c}{c_c} \omega t} \cos \omega t \right] \quad \text{and} \quad (12)$$

$$\ddot{x}_1 = \frac{V_0 \omega}{1+m} \left[e^{-\frac{c}{c_c} \omega t} \sin \omega t \right] \quad (13)$$

when the damping is small. The presence of the terms which have been omitted in the last expressions changes the phase and amplitude of the oscillation to a negligible extent when the damping is kept small.

Expressions for the anvil-table motion are obtainable by going back to the original Equations (1 and 2). Adding these yields

$$M_2 \ddot{x}_2 + M_1 \ddot{x}_1 = 0, \quad (14)$$

from which

$$\ddot{x}_2 = \frac{-V_0 \omega}{1+m} \left[m e^{-\frac{c}{c_c} \omega t} \sin \omega t \right], \quad (15)$$

$$\dot{x}_2 = \frac{V_0}{1+m} \left[1 + m e^{-\frac{c}{c_c} \omega t} \cos \omega t \right], \quad \text{and} \quad (16)$$

$$x_2 = \frac{V_0}{1+m} \left[t + \frac{m e^{-\frac{c}{c_c} \omega t}}{\omega} \sin \omega t \right], \quad (17)$$

the constants of integration being determined from the boundary conditions.

To determine the motions involved as a result of anvil-table reversal, it is simplest to neglect both damping and gravity and to assume that the coefficient of restitution is 0.5.

Let the time of reversal be represented by

$$\tau = \omega t; \quad (18)$$

then the boundary conditions for the new problem can be evaluated from Equations (12), (13), (16), and (17), remembering that the new anvil-table velocity change becomes

$$\dot{x}'_2 = -0.5 \dot{x}_2 \Big|_{t = \tau/\omega} \quad (19)$$

Using Equations (1), and (2), but with $c = 0$, and going through a similar method of solution, the load velocity becomes

$$\begin{aligned} \dot{x}_1 = \frac{V_0}{1+m} [(\sin \tau) \sin \omega t + (1 - \cos \tau) \cos \omega t] + \\ \frac{V_0}{(1+m)^2} \left[m - \frac{1}{2} - \frac{3m}{2} \cos \tau \right] [1 - \cos \omega t] \end{aligned} \quad (20)$$
